

# 5-year chemico-physical evolution of concrete–claystone interfaces, Mont Terri rock laboratory (Switzerland)

Urs Mäder<sup>1</sup> · Andreas Jenni<sup>1</sup> · Cathérine Lerouge<sup>2</sup> · Stephane Gaboreau<sup>2</sup> ·  
Satoru Miyoshi<sup>3</sup> · Yukinobu Kimura<sup>3</sup> · Veerle Cloet<sup>4</sup> · Masaaki Fukaya<sup>3</sup> ·  
Francis Claret<sup>2</sup> · Tsubasa Otake<sup>5</sup> · Masahito Shibata<sup>6</sup> · Barbara Lothenbach<sup>7</sup>

Received: 8 June 2016 / Accepted: 9 December 2016 / Published online: 16 February 2017  
© The Author(s) 2017. This article is published with open access at Springerlink.com

**Abstract** The Cement–Opalinus Clay Interaction (CI) Experiment at the Mont Terri rock laboratory is a long-term passive diffusion–reaction experiment between contrasting materials of relevance to engineered barrier systems/near-field for deep disposal of radioactive waste in claystone (Opalinus Clay). Reaction zones at interfaces of Opalinus Clay with two different types of concrete (OPC and “low-pH”/ESDRED) were examined by sampling after 2.2 and 4.9 years. Analytical methods included element mapping (SEM, EPMA), select spot analysis (EDAX), <sup>14</sup>C-MMA impregnation for radiography, and powder

methods (IR, XRD, clay-exchanger characterisation) on carefully extracted miniature samples (mm). The presence of aggregate grains in concrete made the application of all methods difficult. Common features are a very limited extent of reaction within claystone, and a distinct and regularly zoned reaction zone within the cement matrix that is more extensive in the low-alkali cement (ESDRED). Both interfaces feature a de-calcification zone and overprinted a carbonate alteration zone thought to be mainly responsible for the observed porosity reduction. While OPC shows a distinct sulphate enrichment zone (indicative of ingress from Opalinus Clay), ESDRED displays a wide Mg-enriched zone, also with claystone pore-water as a source. A conclusion is that substitution of OPC by low-alkali cementitious products is not advantageous or necessary solely for the purpose of minimizing the extent of reaction between claystone and cementitious materials. Implications for reactive transport modelling are discussed.

Editorial handling: P. Bossart and A.G. Milnes.

This is paper #15 of the Mont Terri Special Issue of the Swiss Journal of Geosciences (see Bossart et al. 2017, Table 3 and Fig. 7)

✉ Urs Mäder  
urs.maeder@geo.unibe.ch

<sup>1</sup> Institute of Geological Sciences, University of Bern, Baltzerstrasse 3, 3012 Bern, Switzerland

<sup>2</sup> French Geological Survey BRGM, 3 Avenue Claude Guillemin, 45100 Orléans, France

<sup>3</sup> Nuclear Facilities Division, Nuclear Waste Technology Department, OBAYASHI Corporation, 2-15-2, Konan, Minato-ku, Tokyo 108-8502, Japan

<sup>4</sup> National Cooperative for the Disposal of Radioactive Waste NAGRA, Hardstrasse 73, 5430 Wettingen, Switzerland

<sup>5</sup> Division of Sustainable Resources Engineering, Faculty of Engineering, Hokkaido University, Kita 13 Nishi 8, Kita-ku, Sapporo, Hokkaido 060-8628, Japan

<sup>6</sup> Electric and Nuclear Power Technology Department, Taiheiyo Consultant Co. Ltd., 2-4-2, Ohsaku, Sakura 285-0802, Japan

<sup>7</sup> Swiss Federal Laboratories for Materials Science and Technology EMPA, Überlandstrasse 129, 8600 Dübendorf, Switzerland

**Keywords** Concrete clay interaction · Long-term experiment · OPC · ESDRED · Opalinus Clay · Deep geological disposal of nuclear waste

## 1 Introduction

Designs for deep storage of radioactive waste foresee cementitious materials as structural elements, backfill or waste matrix. Interactions take place at interfaces of contrasting materials driven by chemical gradients in pore-water causing diffusive fluxes of dissolved species. This may lead to mineralogical alteration in the barrier system which in turn is expected to locally influence properties like porosity/permeability, swelling pressure or specific retention properties in case of concrete in contact with claystone or compacted bentonite. Laboratory experiments

(Adler 2001; Adler et al. 2001; Dauzères et al. 2010) and in situ experiments (Read et al. 2001; Tinseau et al. 2006; Gaboreau et al. 2011, 2012; Techer et al. 2012; Jenni et al. 2014) demonstrate alteration of both cement paste and claystone adjacent to interfaces. An increase in porosity in the cement paste close to the interface, and clogging in the claystone adjacent to it are commonly predicted by reactive transport modelling (De Windt et al. 2008; Marty et al. 2009; Kosakowski and Berner 2013; Bradbury et al. 2014). Changes in porosity and its distribution—and therefore also permeability—near such interfaces are an important process governing the long-term physicochemical evolution of the engineered barrier and its geological near-field (Kosakowski and Berner 2013; Bildstein and Claret 2015). Clay-rich rocks that are currently under consideration at an advanced stage of repository planning include Opalinus Clay in Switzerland (Nagra 2002), Callovo-Oxfordian “argillite” in France (ANDRA 2005), and Boom Clay in Belgium (SCK-CEN 2012). Clay-based engineered barrier materials include compacted bentonite and sand/bentonite mixtures, among others.

Early efforts (e.g. ECOCLAY-II, European Commission 2005) established a maximum possible extent of deterioration of the clay barrier (worst case) by cementitious materials based on mass balance considerations (Nagra 2002; Mäder and Adler 2005a) or relatively simplistic reactive transport modelling (e.g. Gaucher et al. 2004; De Windt et al. 2004), reflecting limited numerical model capabilities and availability of thermodynamic data. The conclusion was that this “worst-case” extent of degradation (typically some decimeters) would not impact repository performance significantly in clay formations of ca. 100 m thickness (e.g. a key conclusion of ECOCLAY II, European Commission 2005).

More recently, the topic was re-considered in more detail in the context of potential skin effects, whereby a small extent of alteration (e.g. porosity clogging) might have a large impact on gas transport (escaping waste-generated gas) or pore-water transport (e.g. for bentonite saturation) (Kosakowski et al. 2014). In the absence of reliable predictive models, a focus is thus on field studies at repository-like boundary conditions and over time periods in excess of several years, possibly decades. While early work almost exclusively focused on OPC-type concrete (ordinary Portland cement, initial pore-water pH > 13.5), interest in so-called “low-pH” concretes (or low-alkali cementitious products) increased. These low-pH concretes avoid pH values >12.5 [a value buffered by portlandite,  $\text{Ca}(\text{OH})_2$ ] emanating from cementitious materials and thus potentially reduce uncertainty arising from cement interaction at interfaces. Such blends are based on a reduced OPC proportion in combination with addition of a fly ash/slag component and/or reactive silica (silica fume, nanosilica) that promote rapid consumption of portlandite

by hydration to Ca-(Al)-Si-hydrates and ettringite (Ca-Al-sulfate). This will allow pH to drop below 12, typically after some months. Commonly, superplasticizers are required for improved workability, and shotcrete recipes may further include set accelerators, adding dissolved sulphate/aluminate/calcium and possibly also an organic anion component (e.g. formate).

A pioneering experiment with hyperalkaline fluid in Opalinus Clay was carried out at the Mont Terri rock laboratory from 1998 to 2001 that established suitable materials and equipment for circulation systems, electrodes, sampling and analysis of high-pH fluids (Mäder and Adler 2005b). It demonstrated effective buffering of a hyperalkaline fluid by claystone but failed to provide samples of the fluid/claystone interface region due to a technical failure of overcoring. An Mg-layer silicate, calcite and small amounts of Fe-hydroxide were observed as precipitates in the titanium filter sleeve that separated the test interval from the claystone. Associated laboratory batch experiments also did provide insight into some of the expected mineralogical alterations (Adler et al. 1999; Adler and Mäder 1999).

The Cement–Clay Interaction (CI) Experiment carried out at the Mont Terri rock laboratory aims at reducing uncertainties in process understanding related to cement-clay interfaces by providing a detailed analysis of mineralogical changes over relatively long time periods and under realistic boundary conditions. A time frame of at least 20 years is foreseen for the CI experiment, which was installed in 2007. Sampling campaigns were carried out in 2009 and 2012, and most recently in April 2015 (work in progress). This paper summarizes and compares the main findings regarding mineralogy and porosity alterations observed on 2.2 and 4.9 year-old samples at the interfaces between Opalinus Clay and two different types of concrete—an OPC concrete and a low-alkali (low-pH) concrete (named ESDRED). Key issues are a description of the chemico-physical evolution of reaction zones at the interfaces and its consequences for mass transfer in a repository environment, and a comparison of the OPC-claystone and ESDRED-claystone interface region.

## 2 Experimental setup and sampling campaigns

The experiment is located in the HE-D niche adjacent to Gallery-98 that was excavated in 1998 (see overview map in Bossart et al. 2017). This niche is located in the shaly facies of Opalinus Clay (174 Ma marine shale), with a clay content of ~60 wt%.

The field experiment comprises two vertical boreholes (368 mm diameter, up to 9 m deep, BCI-6 and BCI-7 in Fig. 1) in Opalinus Clay, filled each with sections of three different concretes and also a section of compacted

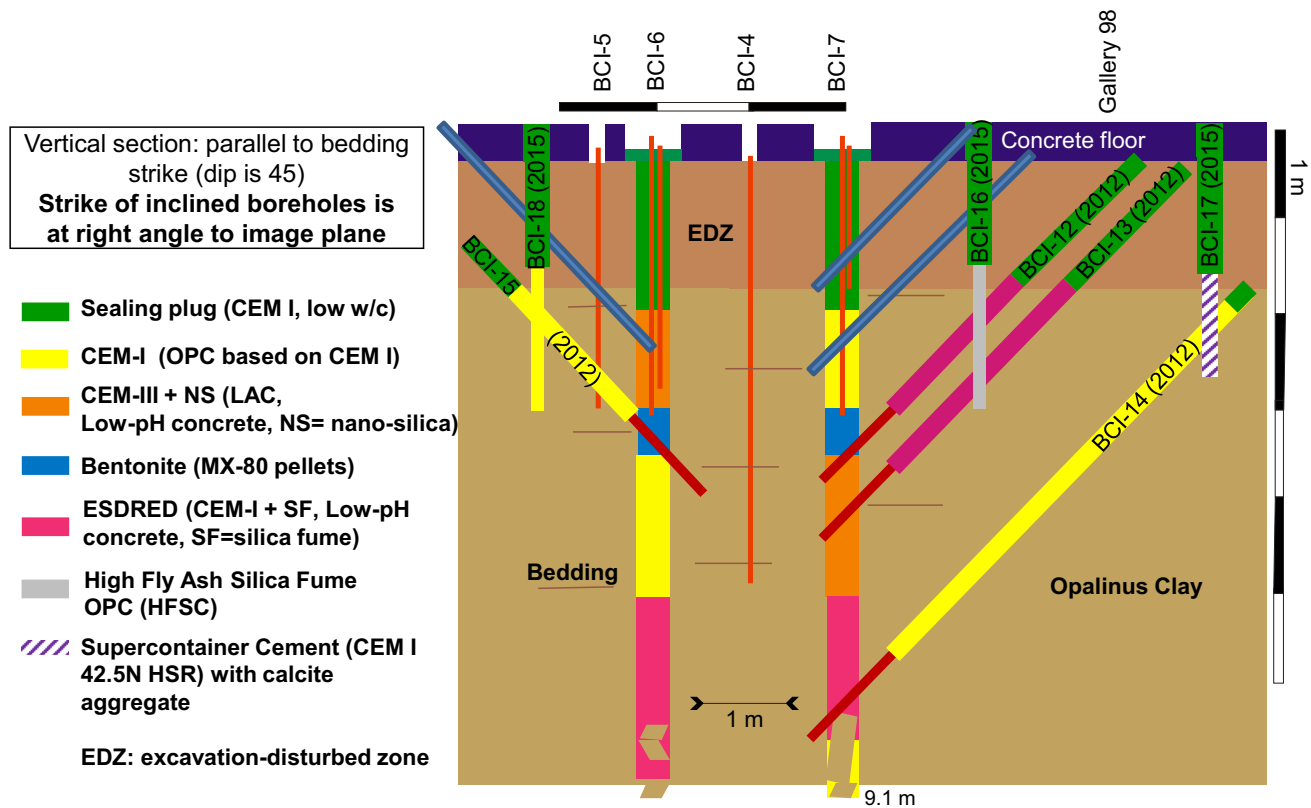


**Fig. 1** Layout of CI Experiment at Mont Terri URL (installed 2007). Dark blue inclined boreholes: first campaign (2009). Yellow and purple inclined boreholes: second campaign (2012). See text for further explanations

bentonite. Two monitoring boreholes (BCI-4 and BCI-5, Fig. 1) record pore-water pressure in Opalinus Clay. In order to compare the effect of different cement types on cement–clay interaction, two types of “low-pH” cement (LAC and ESDRED), and an ordinary Portland cement (OPC) were used to prepare the concrete mixtures. Sections containing compacted bentonite pellets were saturated with a built-in system for injection of artificial pore-water (used for ca. 1 year).

During the past 9 years, three sampling campaigns took place. The first campaign (2009) was carried out after 2.2 years (May and July 2009, boreholes BCI-8, BCI-9 and BCI-10, Fig. 1). The interfaces were stabilized by a small central pilot hole in which a reinforcement rod of either threaded steel or an aluminium tube was cemented in (Fig. 2a). This reinforced section was overcored with a single-barrel 86 mm outer diameter (OD) diamond drilling tool equipped with a core catcher and using a simple Hilti drilling machine and compressed air as cooling agent. This operation was only partially successful, and provided only a limited amount of intact LAC and OPC interface samples (Jenni et al. 2014). The interface between ESDRED and Opalinus Clay was recovered from a mock-up experiment of identical age and material and using the same coring technique (Fig. 2c). The mock-up consists of a 284 mm

diameter core of well-preserved Opalinus Clay encased in concrete and kept sealed in a 100 l drum.

An improved interface stabilization technique was developed for the second sampling campaign in February 2012 (Jenni et al. 2014). It involved drilling an approach borehole of 220 mm OD, drilling of 6 small parallel boreholes (46 mm) across the interface in a circular arrangement with a template, and cementing in of fiber glass rods with epoxy resin (Fig. 2b). Overcoring was then performed through the fiber glass armored palisade of the stabilized sample section with 131/101 mm OD/ID double-barrel equipment containing an acrylic liner for additional protection of the core from air circulation. Perfectly preserved samples of the following interfaces could be obtained: OPC-Opalinus Clay (Fig. 2d) and OPC-Bentonite (borehole BCI-15 in Fig. 1), ESDRED-Opalinus Clay (Fig. 2e, borehole BCI-14 in Fig. 1), as well as LAC-Opalinus Clay and LAC-Bentonite (boreholes BCI-12, BCI-13 in Fig. 1).

A third and currently last drilling campaign took place during April 2015. This campaign sampled the interfaces of the backfilled sampling boreholes from the second campaign (BCI-16 to BCI-18, Fig. 1) that contained mortar and paste of OPC and ESDRED. By backfilling boreholes after sampling, new experiments are generated and it will be

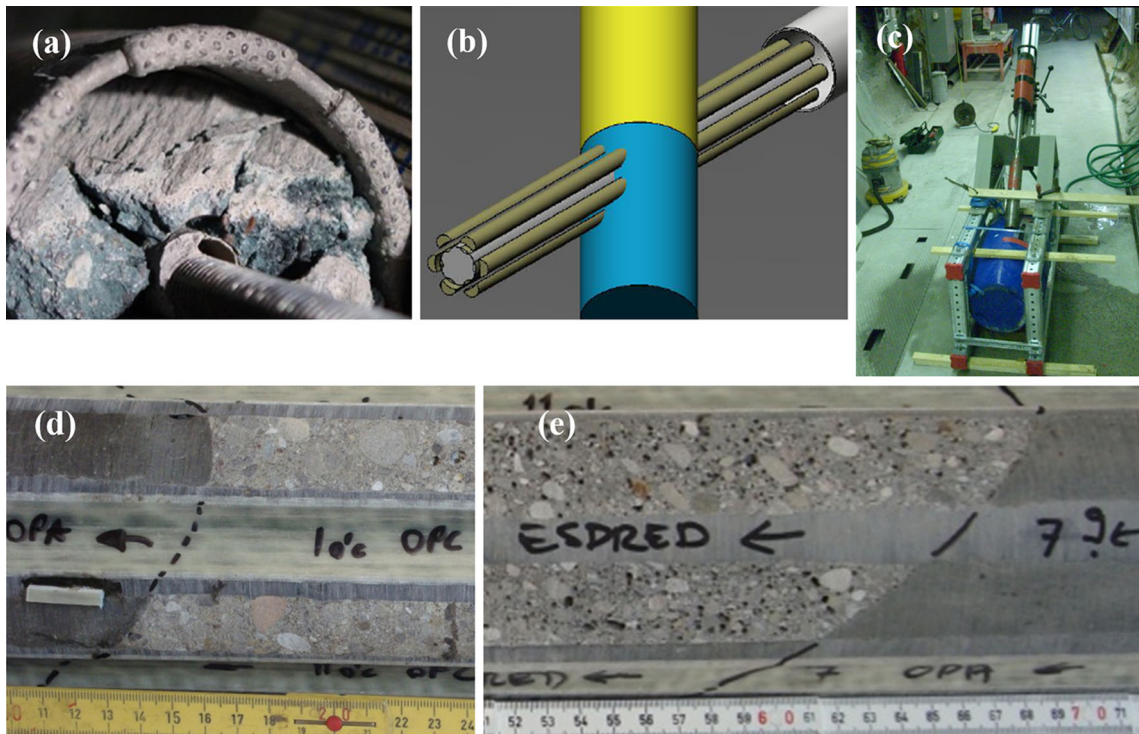


**Fig. 2** Sampling technique: first drilling campaign (a); second campaign (b); drilling of ESDRED sample from mock-up (c); drilled core samples from second campaign (*lower images*): OPC (d) and

ESDRED (e, with abundant former gas pores). *Greenish* material is fibre glass reinforcement

possible to investigate new cement types, or emplace mortar and paste instead of concrete. The backfills of these latest sampling boreholes include OPC, HSFC (high-silica fume/fly ash concrete developed in Japan) and “super-container cement” (CEM I 42.5 N HSR, calcite aggregate, developed in Belgium), a concrete envisaged for high-level radioactive waste containers encased in a concrete shell.

### 3 Materials and methods

#### 3.1 Opalinus Clay

Opalinus Clay of the shaly facies comprises ~60 wt% clay minerals (kaolinite  $\approx$  illite  $>$  illite/smectite mixed layers  $>$  chlorite), ~20 wt% calcite, ~12 wt% quartz, ~3 wt% feldspars, ~2 wt% siderite, ~1 wt% dolomite/ankerite, ~1 wt% pyrite and ~1 wt% organic carbon (Pearson et al. 2003; Jenni et al. 2014). The average porosity is 16% (water content of ~6.4 wt%), and the pore-water composition at this location contains ca. 8.4 g/l chloride, 1.13 g/l sulphate, 4.7 g/l sodium, 0.5 g/l calcium, 0.34 g/l magnesium, and 0.022 g/l bicarbonate, a composition adjusted to 10% lower salinity from Koroleva et al. (2011) at the well-studied nearby PC location (see also Table 1). The cation exchange capacity (CEC) ranges from

80–180 meq/kg dry rock depending on clay content (Pearson et al. 2003), and the occupancy is approximately 0.52, 0.21, 0.18, 0.08, 0.01 in equivalent fractions for Na, Ca, Mg, K, Sr, respectively, at the nearby PC location (Koroleva et al. 2011). Samples from the CI location averaged ~120 meq/kg rock for CEC (Jenni et al. 2014, and details below). The clay exchanger includes an inventory of readily available cations of ~120 meq/kg dry rock (260 cation meq/kg<sub>pw</sub>, 6.4 wt% pore-water) that exceeds the pore-water inventory by a factor of ~7. Illite, illite/smectite mixed layers and kaolinite also contain amphoteric edge sites that can be protonated or deprotonated, and form a pH buffer capacity that may retard the leading (dilute) edge of a high-pH front, for example. The capacity was estimated to be about 0.25% of the CEC, ~0.3 meq/kg, based on a fairly complex derivation from experimental measurements on illite (Bradbury and Baeyens 2000, 2005).

#### 3.2 Concretes (OPC, ESDRED) and cement hydration

The compositions of the two different concrete mixtures are provided in Jenni et al. (2014), including organic additives, and aggregate <16 mm. The main difference between the OPC (CEM I 42.5 R HS) and the low-alkali

**Table 1** Approximate initial pore-water concentrations and direction of chemical gradients

Material	Age range	$\text{Ca}^{2+}$	$\text{Mg}^{2+}$	$\text{Na}^+$	$\text{K}^+$	$\text{SO}_4^{2-}$	$\text{Cl}^-$	$\text{CO}_3^{2-}$	$\text{OH}^-$
OPC	0.04–1310	24–2.9	<	26–90	137–209	66–4.5	<	~0.05	>200
ESDRED	0.04–1310	9.2–29	0–0.005	100–22	186–11	2–1.8	<	~0.05	180–7*
Gradient		↑↓ - ↓↑	↑↑	↑↑	↓↓	↑↓ - ↑↑	↑↑	↑↑	↓↓
OPA		12.7	14.3	204	2.3	11.8	237	~0.4	$\sim 10^{-7}$

Concentrations in mmol/l; age range in days; < indicates below detection; first arrow (or pair) indicates direction of gradient at early time, second arrow at later times; long arrow is for ESDRED, short arrow for OPC

<sup>a</sup> Formate is also significant as anionic charge carrier

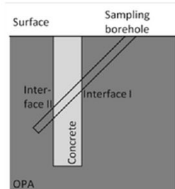
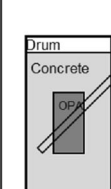
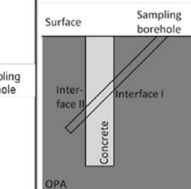
cementitious product ESDRED (CEM I 42.5 N) is the presence of a substantial amount of silica fume, superplasticizer and set accelerator in the latter. ESDRED was originally developed as a low-pH shotcrete (Alonso et al. 2009). The available samples and their provenance, age and key cement characteristics are summarized in Fig. 3. The interface between ESDRED and Opalinus Clay after 2.2 years was substituted from a mock-up sample cast at the same time as the experiment was installed (Fig. 2c, e). The water/binder ratio of the OPC sample collected after 2.2 years taken from the sealing plug was distinctly lower (0.35) than that used for the OPC sections (0.8) sampled after 4.9 years. Both substitutions were made necessary due to technical difficulties during the first campaign in obtaining samples of sufficient quality. A special feature of the ESDRED concrete is the use of a set accelerator, containing mainly aluminate, sulphate and formate (Andersson et al. 2008; Lothenbach et al. 2014; Wieland et al. 2014).

ment hydration (closed system) was studied experimentally in detail with support from this project and also including thermodynamic modelling of hydration progress. Details and data for the ESDRED mix were published by Lothenbach et al. (2014), Lothenbach (2013) and Wieland et al. (2014), the latter with focus on superplasticizers and its role on radionuclide uptake. OPC hydration and its modelling was published by Lothenbach and Winnefeld (2006) but this was based on a somewhat different cement composition than the one used here, CEM I 42.5 R HS. Experimental results are included in the “Appendix”, adapted from an unpublished Mont Terri Project technical note (Lothenbach 2011).

### 3.3 Methods

Polished sections and thin sections across the concrete-Opalinus Clay interface were prepared without water contact to avoid rehydration of remaining clinker phases in

**Fig. 3** Properties of OPC and ESDRED cement, water/binder ratio, and pictograms of sample provenance.  $\text{C}_3\text{A}$ : tricalcium silicate contained in clinker

	<b>OPC-OPA</b>		<b>ESDRED-OPA</b>	
cement	CEM I 42.5 R HS		CEM I 42.5 N	
	low $\text{C}_3\text{A}$ (sulfate resistant)		40% of cement substituted with silica fume	
age	2.2 y	4.85 y	2.2 y	4.85 y
water/binder	0.35	0.80	0.50	
origin	in-situ 		drum	in-situ
				

the cement and dissolution of cement hydrates, and to suppress the swelling of clay minerals and pyrite oxidation in Opalinus Clay. Large differences in hardness and the mechanically weak interfaces posed additional challenges for sample cutting and handling. The samples were first embedded in resin, then the surface to be analysed was chosen at 45° or 90° to the interface plane, and cutting was done with a small diamond saw using petroleum as lubricant. The cut surface was processed using sand paper, oil-based diamond suspensions and petroleum.

Analytical methods except for EPMA (electron probe micro analysis) are described in detail in Jenni et al. (2014) and cater to the fine grained nature of the materials (Opalinus Clay, hydrated cement matrix) and the expected small-scale (mm to  $\mu\text{m}$ ) multiple mineral alteration zones. In short, the following tools were applied: (1) SEM/EDAX imaging, element mapping and spot analyses in low vacuum mode (University of Bern), (2) transmission light microscopy on polished thin sections, also used for element mapping (University of Bern), (3) EPMA mapping on a JXA-8100 of JEOL (15 keV,  $20 \times 20 \mu\text{m}$  and  $2 \times 2 \mu\text{m}$  beam size, 40 ms per spot, Obayashi Corp./Taiheiyo Consultant Co.), (4)  $^{14}\text{C}$ -doped polymethylmethacrylate (PMMA) impregnation followed by radiography polished surfaces (BRGM), (5) scraping out miniature powder samples from cement matrix and Opalinus Clay for (6) IR measurements, (7) powder XRD, and (8) determination of exchangeable cations and cation exchange capacity (CEC) by the Co-hexammine trichloride method (BRGM), (9) powder XRD on a RIGAKU RINT2500 on thin (mm) slices of sample (Obayashi Corp./Hokkaido University). Synchrotron beamline powder  $\mu$ -XRD on polished thin sections ( $5 \mu\text{m}$ ) on  $200 \mu\text{m}$  thick optical glass carriers (details in Dähn et al. 2014) is selectively quoted, but data has not yet been fully processed.

### 3.4 Analytical issues and phase identification

Both, cement matrix and clayey matrix do not permit spot analyses (composition, spectroscopy, structure) of pure phases but deliver a signal from a mixture of phases. Resolving such mixtures remains a challenge specifically in case of the presence of amorphous or poorly crystalline phases (e.g. Ca–Si-hydrates, Mg–Si-hydrates, amorphous silica). Element maps combined with spatially resolved methods (EDAX, FTIR,  $\mu$ -XRD, etc.) are a powerful tool to characterize major bulk mass transfers and some phase identities. This would be the type of information required also for a modelling approach: the scale of alteration, quantitative or semi-quantitative information on mass transfers, and identity or at least restrictions on the participating primary and secondary phases. Further efforts, specifically including  $\mu$ -XRD are presently on-going. A

quantification of spatially resolved total porosity is also a key issue. Most common methods are hampered by artefacts from sample preparation or by the presence of a large portion of nano-scale and micro-scale porosity. The method applied here using impregnation of  $^{14}\text{C}$ -labelled PMMA combined with radiography is thought to be best suited (Gaboreau et al. 2011). The acrylic monomer is a small molecule, mixes with water and has been shown to also penetrate clay-interlayers of smectites (Prêt et al. 2004; Massat et al. 2016). While the pore-geometry cannot be resolved at the relevant small scale, a quantification of local bulk porosity by radiography is possible (quantification involving post-processing of images and calibration is ongoing).

## 4 Results and discussion

Results of sample analysis from interfaces after 2.2 years were presented in detail by Jenni et al. (2014). Dauzeres et al. (2016) presented details of interfaces between another type of low-alkali cement (LAC) and Opalinus Clay and ESDRED-Opalinus Clay, with focus on the concrete part and Mg–Si-hydrates. Here, we focus on the OPC and ESDRED samples collected after 4.9 years in direct comparison to the samples from the earlier campaign, aiming at a comparison between OPC and low-pH concrete behaviour, and also detailing the claystone part.

### 4.1 Chemical gradients across interfaces

Transport of dissolved species across the claystone-concrete interface is driven by differences in chemical potentials between the two contrasting pore-waters, and its evolution with time (Table 1, modified from Jenni et al. 2014; ESDRED: Lothenbach 2013, Lothenbach et al. 2014; OPC: “Appendix”). Key gradients in concentrations are opposite for Na and K, large and opposite for Cl and OH, and distinct for Mg and dissolved carbonate from claystone into concrete. Sulphate is being consumed (strongly so in ESDRED) during cement hydration and this leads to a reversal of gradients with time. The gradient in Ca is opposite between OPC (initially high) and ESDRED (initially low) and reverses during hydration. The pore-water evolution in concrete during hydration indicated in Table 1 is valid for closed systems (Lothenbach and Winnefeld 2006; Lothenbach et al. 2014; “Appendix”) but will be different near the interface where dissolved components will exchange with Opalinus Clay and/or are controlled by solubility with respect to different secondary phases than observed in a closed cement system. Specifically, pH may drop due to mineral dissolution (and precipitation) reactions, rather than stay above 13 (OPC) or drop below 12

(ESDRED) after ca. 100 days, as seen during hydration in a closed system. The concentrations of dissolved silica in the hydrating cements are somewhat higher or similar to Opalinus Clay pore-water, and dissolved Al concentrations are about an order of magnitude smaller than Si concentrations. Major components associated with large gradients are therefore  $\text{OH}^-$ ,  $\text{Cl}^-$ ,  $\text{SO}_4^{2-}$ ,  $\text{Na}^+$ ,  $\text{K}^+$ ,  $\text{Ca}^{2+}$  and  $\text{Mg}^{2+}$ .

More than a third of the anionic charge is initially carried by formate rather than  $\text{OH}^-$  in ESDRED concrete, and formate dominates as charge carrier at later hydration times (Lothenbach et al. 2014). Alkalies diminish rather rapidly in ESDRED concrete after mixing with water, presumably due to incorporation into Ca–Si-hydrate with low Ca/Si, whereas alkalies remain in OPC pore-water during hydration in a closed system (high Ca/Si-ratio Ca–Si-hydrates do not readily incorporate alkalies).

## 4.2 OPC-Opalinus Clay interface

### 4.2.1 Zoned interface region: element maps and XRD

The major characteristics (Table 2) of the 2.2- and 4.9-year interfaces were derived from SEM/EDAX images (Figs. 4, 5) and photomicrographs (not shown). Note that bedding trends are inclined at about  $45^\circ$  to the interface, marked for example by shrinkage cracks, best seen on the large-scale false-colour EPMA element maps. The difference in water/binder ratio (w/b) complicates direct comparison of 2.2- and 4.9-year interface characteristics. The very low w/b = 0.35 in case of the 2.2-year sample (sealing plug, Fig. 1) is expected to yield very low capillary porosity in the cement matrix that might significantly reduce diffusive transport. The thicker interaction zones observed after 4.9 years (e.g. sulphur enrichment, carbonate alteration) cannot be attributed solely to longer interaction time, but also to a faster diffusive transport due to a much larger porosity in this w/b = 0.80 OPC. Some specific features

seen in the 2.2 year-old altered cement (details below) are explained by a shortage of water during the earliest hydration stage: despite all precautions, the OPA borehole walls are expected to dry slightly before concrete casting. As soon as the concrete was emplaced, water might have been sucked into the dry margin of OPA and hindered cement hydration. With time, pore-water pressure increased again (as observed in a nearby test interval in Opalinus Clay), and pore-water from claystone was supplied to the cement, leading to a secondary hydration and conversion of remaining alite (Ca-silicate clinker phase) into an otherwise uncommon Mg-hydrate. Carbonate formation in the cement matrix caused by the bicarbonate-rich claystone pore-water further slowed down this secondary hydration by porosity reduction, and a zone of unhydrated clinker remained. This mechanism is considered a special case caused by the low water content of the 2.2-year OPC sample (sealing plug), and this added complexity may not have been experienced by the OPC sampled after 4.9 years, a likely explanation for the simpler zoning pattern observed in this sample, and a lack of evidence for two separate hydration stages.

Zonation of mineral alteration within the cement matrix for 2.2-year samples is detailed in Jenni et al. (2014) and it is also supported by numerous spot EDAX analyses (zone labels refer to Fig. 4, top left):

C1: Ca-rich margin, not continuous, carbonated, unhydrated ferrite, alite transformed to Mg–Al-phase (hydrotalcite?).

C2: Ca-depleted relative to bulk, carbonated, unhydrated ferrite, alite transformed to Mg–Al-phase (hydrotalcite?).

C3: elevated S and increasing Ca (but depleted relative to bulk), not carbonated, Ca-rich patches (portlandite), unhydrated ferrite, alite transformed to Mg-phase (hydrotalcite?).

**Table 2** Summary of characteristics at the OPC-Opalinus Clay interface after 2.2 (2) and 4.9 (5) years

	[ $\mu\text{m}$ ] [years]	Ca 2   5	Mg 2   5	S 2   5	carbonation 2   5	alite & belite 2   5	Mg hydrate 2   5
OPA	-200	+	(+)	(+)	Unaltered		
OPC	0	-   -		(+)	✓		✓
	300			+		✓	
	800			+		✓	
	3000				Unaltered		

Empty cells: same characteristics as unaltered material. Approximate thickness of layers in  $\mu\text{m}$  is indicated

+, -, ✓ represent “enriched”, “depleted”, and “present”, relative to the unaltered OPA or cement far from interface. (+): Small enrichment

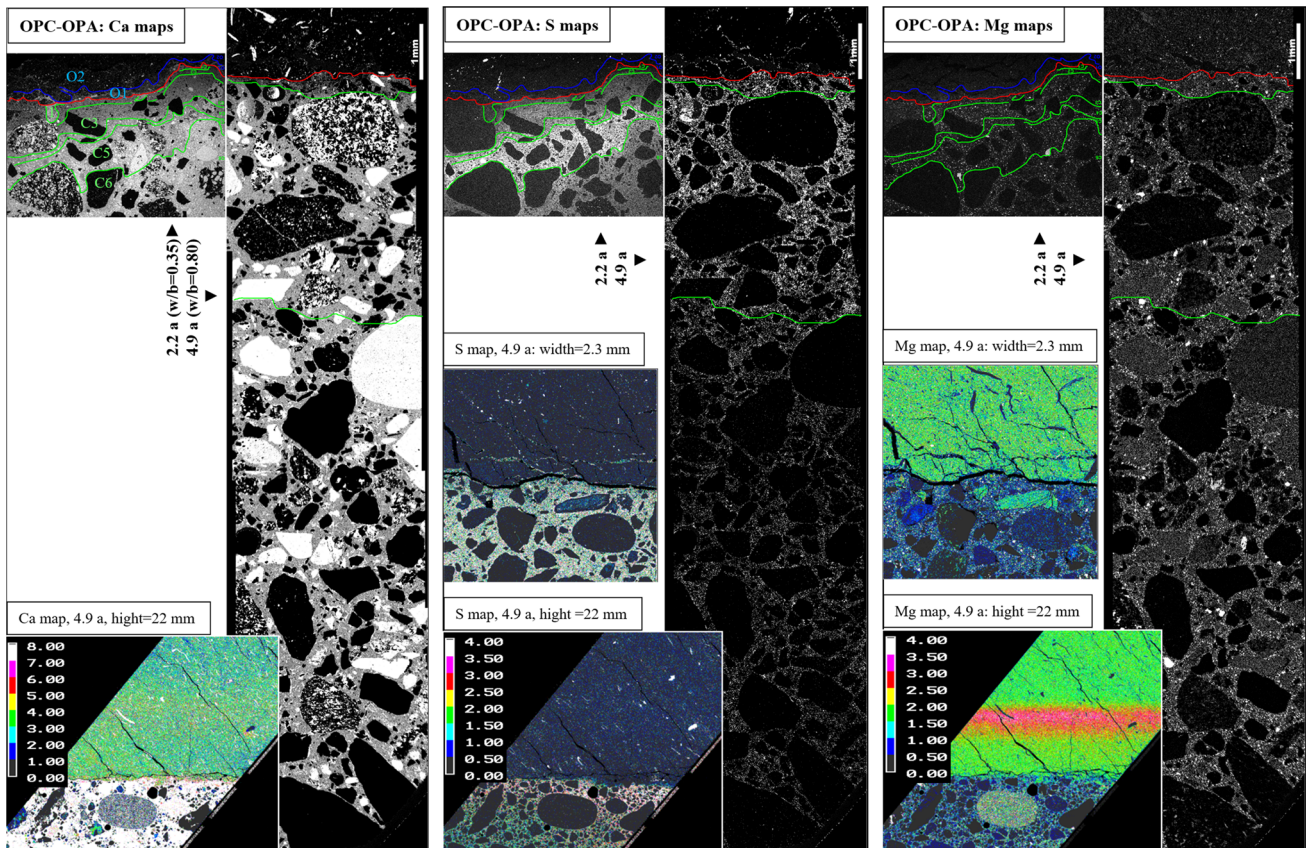


**Fig. 4** SEM-EDAX element maps (grey-scale) of Ca (left), Mg (centre), S (right) of 2.2-year samples (small areas) and 4.9-year samples (merged long maps). False-colour inserts are from EPMA element maps in oxide wt% from 4.9-year samples (small and large

areas). The interface OPC-Opalinus Clay is marked in red (SEM maps) or is a resin-filled discontinuity (EPMA). See text for explanation of zones in cement matrix (green lines) and in Opalinus Clay (blue line)

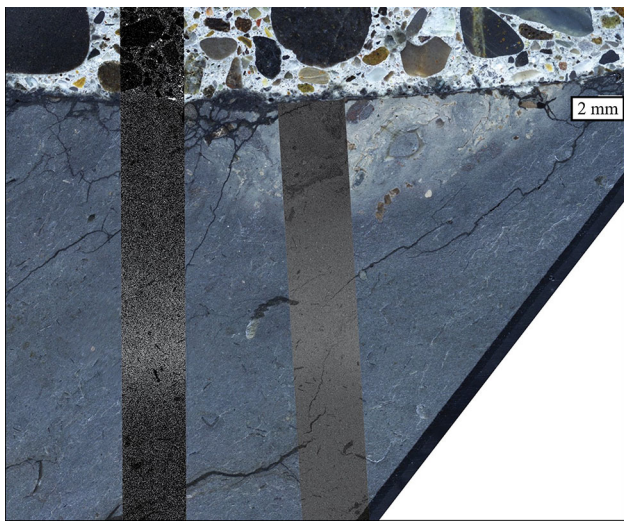


**Fig. 5** SEM-EDAX composite Mg-maps (greyscale stripes) superimposed on reflected-light image of interface between OPC concrete (top) and Opalinus Clay. A *buff coloured* region bordering the interface is rich in phosphate (fossil debris). The width of the image is 26 mm

C4: *Ca similar to bulk, increase in S with distance, relict clinker grains, Al-rich domains (ettringite, monosulphate).*

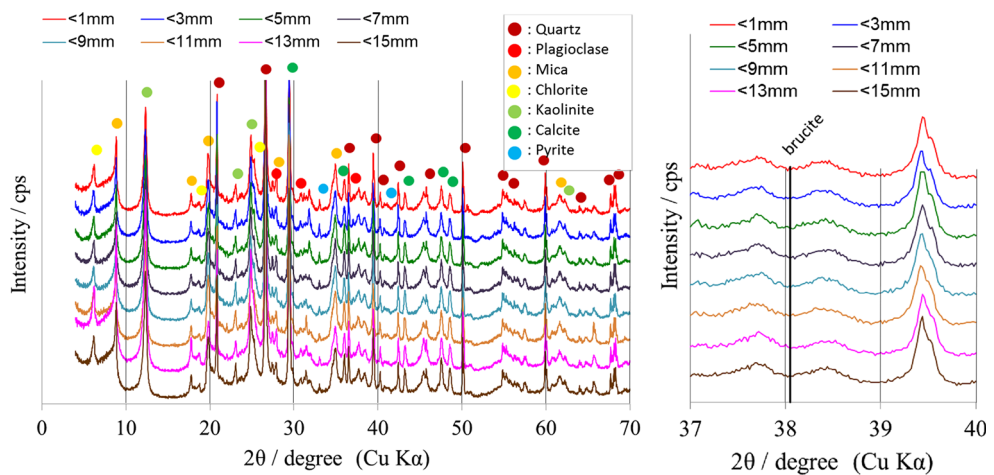
C5: *max. S content, Ca above bulk value, Al and Mg-rich patches, increased hydration of clinker.*

C6: *similar to C5, lower S and more hydrated, similar to a “normal” OPC.*

The features on the concrete side of the interface that are thought not to be influenced by inferred de-saturation and secondary hydration effects (italicized in the list above) include (1) a carbonate-containing margin, locally Ca-enriched right at the interface but Ca-depleted for the most part (100–300 µm), (2) a zone with bulk Ca-content and somewhat elevated sulphur (200–300 µm), and (3) a sulphur-enriched zone (500–1000 µm).

In contrast, the concrete margin observed after 4.9 years is chemically less zoned (Fig. 4; Table 2) and the clinker is fully hydrated (except for minor relict Ca-ferrite), without detectable Mg-rich phases. The extent of the carbonate containing zone is more difficult to distinguish and associated with a Ca-depleted zone (100–300 µm), similar in

**Fig. 6** XRD patterns obtained from a profile in Opalinus Clay adjacent to OPC (4.9 year) with 2 mm spatial resolution. *Blow-up* shows region of interest for possible Mg-hydroxide (brucite)



width as observed after 2.2 years. The sulphur-enriched zone is much wider ( $\sim 4000 \mu\text{m}$ ) compared to 2.2 years, and slightly Ca-depleted at its proximal margin.

The regions where SEM-EDAX element mapping was performed were duplicated and extended by EPMA element mapping on a different 4.9-year core samples. The same wide sulphur-rich zone was observed, but shown more quantitatively in oxide wt% of Ca, Mg and S in false colour images (Fig. 4). Likewise, Ca concentrations measured by EPMA (not visible in Ca map, above range of scale) gradually increase in concrete from 20 to 30 wt% CaO over 7–8 mm from the interface, but remain constant at 4 wt% in the claystone.

There is little evidence for chemical interaction on the claystone side (Fig. 4; Table 2) close to the interface. A narrow zone somewhat enriched in Ca with slightly elevated sulphur is seen after 2.2 years (100–200  $\mu\text{m}$ ), but none after 4.9 years, except for some tiny mineralized veinlets that are thought to be associated with a narrow borehole disturbed zone.

The false-colour EPMA Mg-map reveals a striking Mg-enriched zone in the claystone at a distance of 4–6 mm from the interface (not covered by SEM-EDAX maps). The enrichment is ca. 1 wt% MgO from a background value of 2 wt% to ca. 3 wt% in the enriched zone. This Mg zone was also confirmed in a different sample with two extended composite SEM-EDAX maps extending deeper into the claystone (Fig. 5). A Mg-enriched zone is located at ca. 6–8 mm distance from the interface, regardless of rather large heterogeneities in phosphate contents (details on this lithology below). Attempts failed to detect a mineral phase associated with this Mg-enrichment by XRD. A well resolved (2 mm) XRD profile (Fig. 6) did show very little variation in mineral proportions and no newly-formed phases. Specifically, brucite as a likely candidate Mg-phase could not be detected.

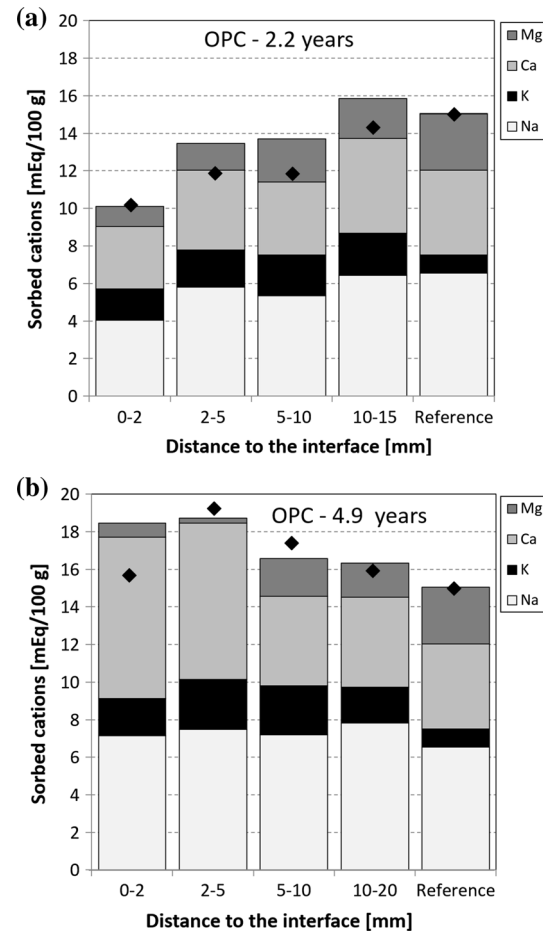


**Fig. 7** CEC (diamonds, meq/100 g) and cation occupancy (meq/100 g) on clay exchanger in Opalinus Clay as function of distance from the interface to OPC, after 2.2 (a) and 4.9 years (b)

#### 4.2.2 Zoned interface region: exchangeable cations in Opalinus Clay

Very small samples of powdered claystone were analysed for its cation exchange capacity (CEC) and cation

occupancy (Na, K, Ca, Mg, Sr), but at a coarser spatial resolution (up to 20 mm distance from interface) compared to the SEM/EPMA work presented above. A Mg-depleted zone is evident in the 2.2-year sample from 0 to 5 mm of the interface (or smaller), and relatively little variation in cation occupancy and CEC from there onwards (Fig. 7a). Potassium is relatively enriched up to the limit of measurement at 15 mm distance compared to a more distant bulk sample (reference). After 4.9 years, a Ca-enriched and Mg-depleted zone extends to ca. 5 mm (Fig. 7b). There is generally a somewhat larger error associated with analytical protocols optimized for such small samples, but the qualitative trends are valid.

#### 4.2.3 Effect of phosphate-rich lithology

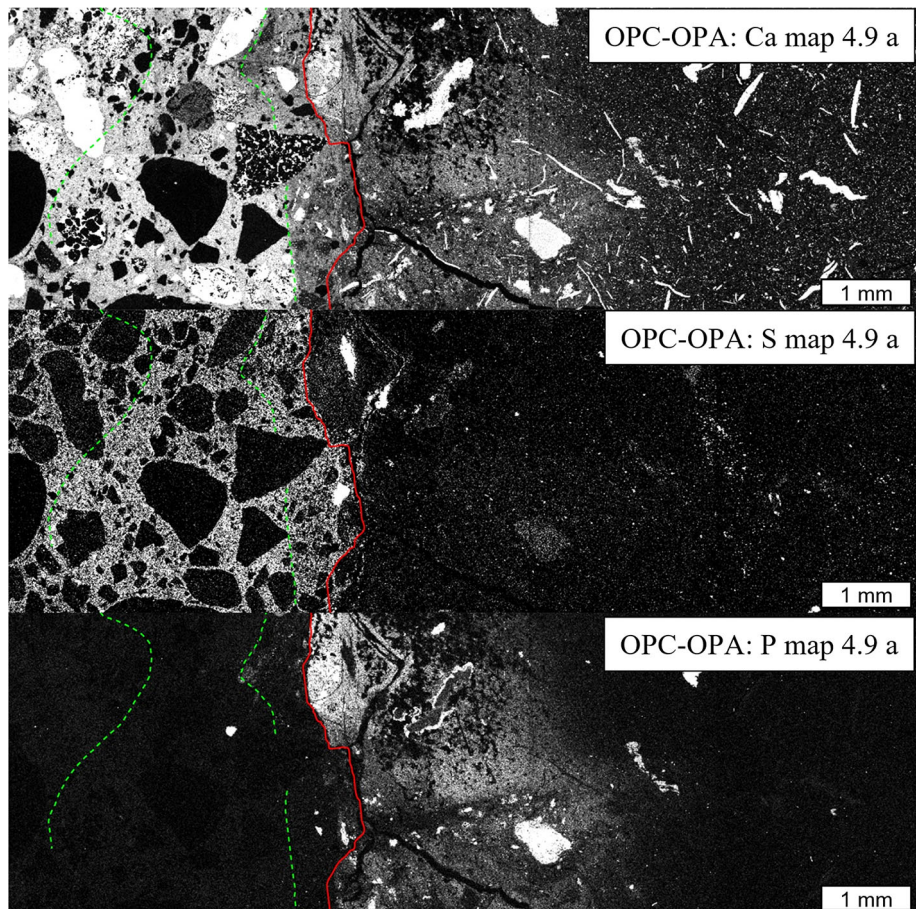
An unusual accumulation of fossil shell fragments in Opalinus Clay exactly at the OPC interface where the 4.9-year sample was taken provided an increased source for S, Fe, and P (Figs. 5, 8). An increased amount of pyrite accumulations (S map; Fe map not shown) was associated with a significantly increased P-content in the clay matrix as well as P-rich particles (P map). Apatite was also identified in the cement matrix by  $\mu$ -XRD in case of this

specific sample ( $100 \mu\text{m}^2$  beam, work in progress, method in Dähn et al. 2014), indicating that phosphate was mobile and interacted with the cement. The increase of sulphur in the clay matrix (other than associated with pyrite) suggests that a partial oxidation of pyrite was a source for mobile sulphate, also supported by earlier findings (Jenni et al. 2014) where oxidized surfaces of pyrite were documented. This additional sulphate might also have contributed to a larger thickness of the sulphur-enriched layer in concrete in the 4.9-year sample compared to the one after 2.2 years. It is believed that this limited pyrite oxidation occurred during/after drilling the experiment borehole by limited access of oxygen and stopped after concrete casting and oxygen consumption.

#### 4.2.4 Porosity changes across interface region

Porosimetry analysis of the OPC-Opalinus Clay interface after impregnation with  $^{14}\text{C}$ -doped MMA resulted in the autoradiograph shown in Fig. 9. Brighter regions represent lower porosity for the 2.2-year samples (less blackened negative film). Segmentation of the concrete part (exclusion of aggregates, cracks and claystone, all shown in black) revealed an obvious zone of lower porosity parallel

**Fig. 8** Ca, S, and P SEM-EDAX maps of a section across the OPC-Opalinus Clay interface, 4.9 years after emplacement. Different zones in cement are separated by green lines (see text), the cement/claystone interface is traced in red



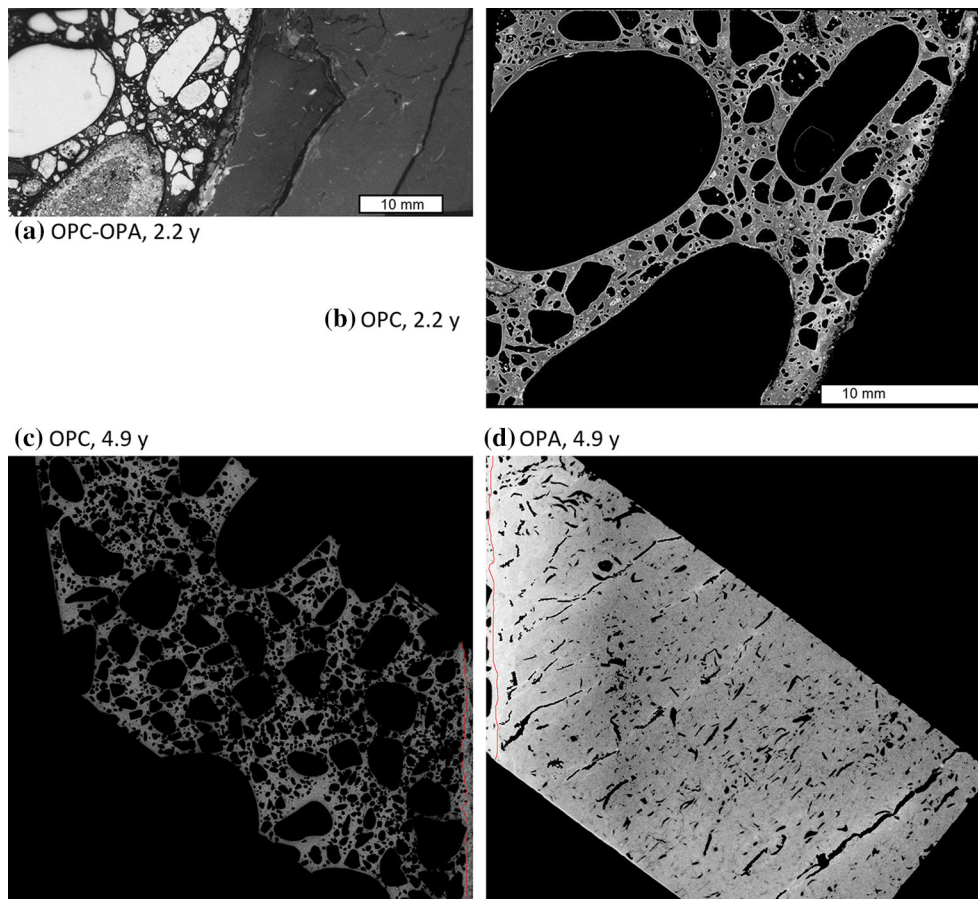


**Fig. 9** Autoradiographs of the OPC-Opalinus Clay interface after 2.2 and 4.9 years. Untreated autoradiograph (**a**, 2.2 year) and processed concrete side of the autoradiograph (**b**). Processed concrete side (**c**,

4.9 year) and processed claystone side (**d**, 4.9 year). The width of the rectangular samples is 22 mm. The interface is marked with a red line

to the interface within the cement matrix, but not directly adjacent to it (Fig. 9b). The thickness of this zone is approximately 1.2 mm, and it is largely coincident with the location of carbonate alteration. The same image treatment applied to the 4.9-year sample (Fig. 9c), but here in reversed grey scale (bright areas are porous) does show less variation in porosity. The claystone side (Fig. 9d) shows somewhat elevated porosity towards the interface but this may also be a result of a mechanically induced drilling-disturbed zone from drilling of the emplacement borehole. MMA-filled cracks induced by sample drying (preferentially parallel to bedding) and fossil fragments with nearly no porosity were segmented and are shown in black. There appears to be a slightly less porous zone at ca. 8–10 mm distance from the interface, and this may correlate with the Mg-enriched zone documented above (Fig. 4).

#### 4.3 ESDRED-Opalinus Clay interface

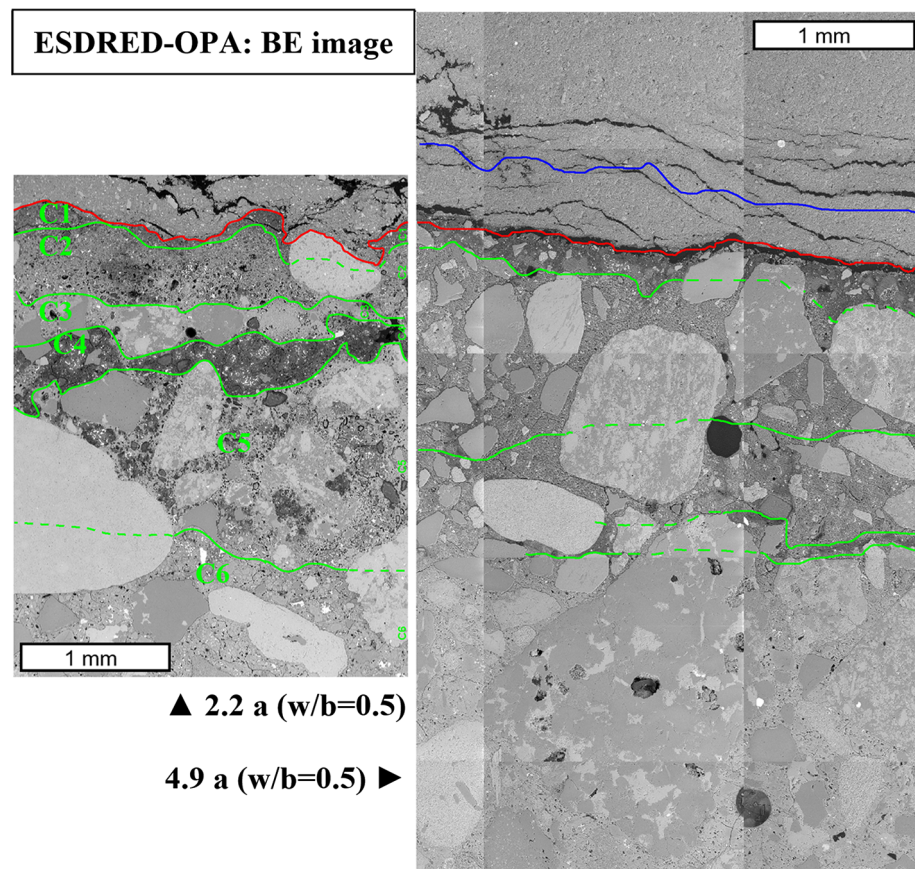
Dauzeres et al. (2016) examined the interfaces between LAC-Opalinus Clay on 4.9-year samples, but also those of ESDRED-Opalinus Clay, with focus on Mg-Si-hydrates

that formed in the cement matrix of both types of “low-pH” concretes close to the interface with claystone. For ESDRED, a ca. 3 mm wide Mg-enriched zone along a 30 mm long interface sample was shown on SEM-EDAX composite element maps that coincided also with a Ca-depleted zone. Small powder samples from this zone were examined by  $^{29}\text{Si}$ -MAS-NMR and FTIR and the Mg-bearing phase was identified as mainly Mg-Si-hydrate, also in analogy to spectra obtained from recent characterisation of synthetic Mg-Si-hydrates (Lothenbach et al. 2015; Roosz et al. 2015; Nied et al. 2016). Below, we complement this work and provide also details on the alteration observed on the claystone-side of the interface.

##### 4.3.1 Zoned interface region: element maps

The quality of sample preparation is illustrated in Fig. 10 (back-scattered electron image), where discrete shrinkage cracks in claystone developed during freeze-drying of the sample, but otherwise perfectly polished surfaces represent a section free of artefacts. Also visible is a much higher content of initial gas pores in this shotcrete mix design (a

**Fig. 10** SEM back-scattered electron images of ESDRED-Opalinus Clay interface region (2.2 and 4.9 years). See text for explanation of zones. Red line marks the interface. Opalinus Clay is at the top. The width of the right composite image is 3 mm, the width of the left image 2.3 mm



fairly viscous shotcrete recipe) compared to OPC. Interpretation focuses solely on the clay-rich matrix and the hydrated cement matrix, omitting fossil fragments, silt and aggregate grains.

Compared to OPC, the ESDRED cement matrix contains up to twice the proportion of Si in all zones due to the addition of silica fume. Jenni et al. (2014) distinguished the following zones in a 2.2-year sample (Figs. 10, 11).

C1: contains unhydrated ferrite skeletons; Mg-hydrate replacing alite and belite (Ca-silicate clinkers); Ca-depleted zone; carbonate alteration.

C2: contains unhydrated ferrite skeletons; Mg-hydrate replacing alite and belite; Ca-depleted; carbonate alteration.

C3: most Ca and S enriched zone; almost no ferrite and Mg-hydrate; carbonate alteration.

C4: lowest Ca and S, but highest in Mg; ferrite present; Mg-hydrate abundant; carbonate alteration.

C5: patches of portlandite; patches high in Si; some Mg-hydrate; some relict ferrite and aluminate; carbonate alteration.

C6: less portlandite and Mg-hydrate; some relict belite; close to bulk unreacted cement.

The altered zone in concrete after 4.9 years is similar in width (Fig. 11) but with a slightly simpler zoning pattern

compared to the 2.2-year sample. An almost 2 mm wide Ca and S depleted zone (C1-C5 in Fig. 11) is only slightly wider than a Mg-enriched zone (most Mg-rich in C2-C3, less so next to OPA, C1). Alite and belite were fully hydrated after 4.9 years, and a distinct Ca-Mg-poor but sulphur-rich intermediate zone (C4, 2.2 years, Fig. 11) is not observed.

A distinct and ca. 0.5 mm wide Mg-enriched zone developed in the claystone close to the interface (Fig. 11) after 2.2 and 4.9 years. Other than this, Opalinus Clay appeared unaltered at the resolution of element mapping and XRD (Jenni et al. 2014, Dauzères et al. 2016). A summary of the alteration zones developed after 2.2 and 4.9 years is given in Table 3. Observations on the degree of enrichment or depletion are additionally supported by numerous EDAX spot analyses (details of 2.2-year samples in Jenni et al. 2014, element-ratio data for 4.9-year sample in Dauzères et al. 2016).

#### 4.3.2 Zoned interface region: exchangeable cations in Opalinus Clay

A zone of ca. 0.4 mm width and enriched in Mg was observed after 4.9 years (Fig. 11, Mg maps), and this zone correlates with elevated Mg seen also on the exchanger

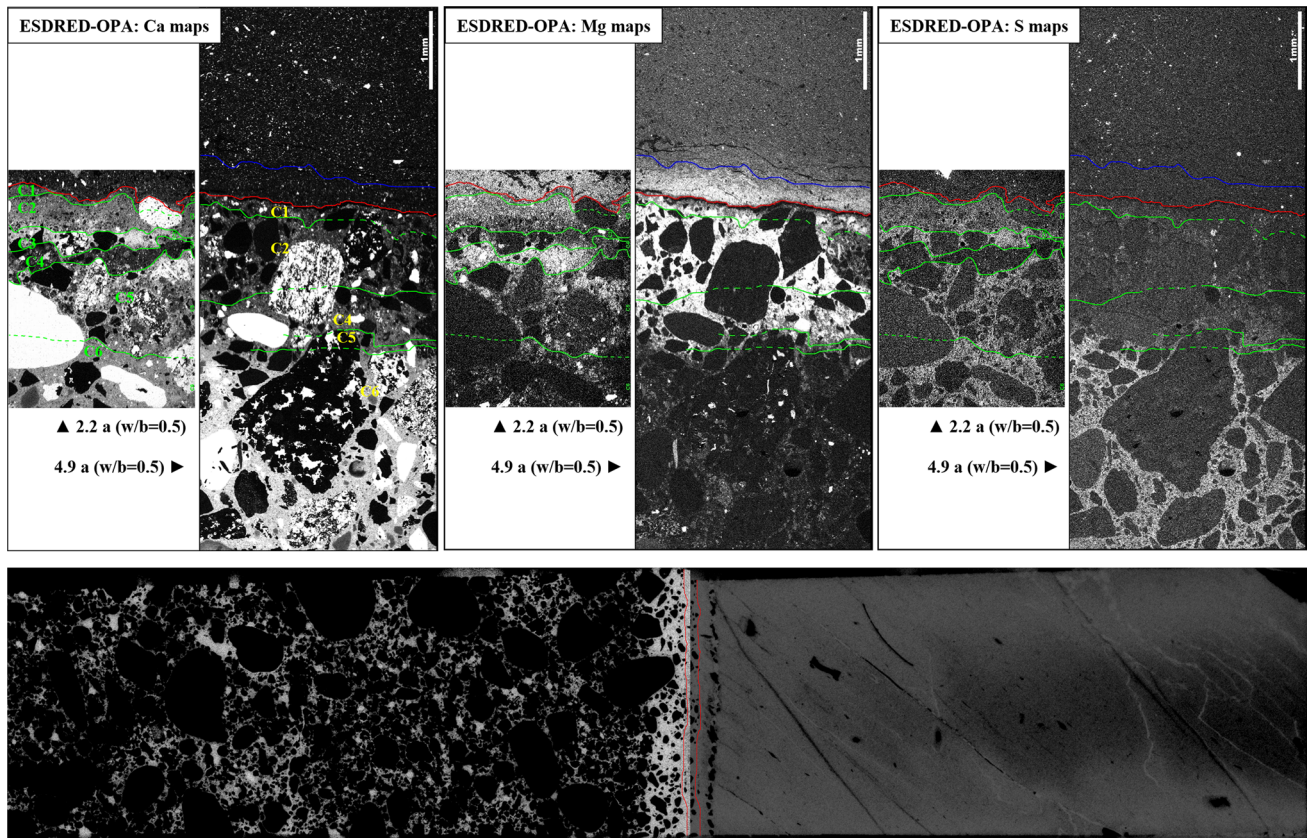


**Fig. 11** SEM-EDAX element maps (grey-scale) of Ca (left), Mg (centre), S (right) of 2.2-year samples (smaller areas) and 4.9-year samples (merged long maps). The interface OPC-Opalinus Clay is marked in red. See text for explanation of zones in cement matrix

(green lines) and in claystone (blue line). Lower images radiographic images of  $^{14}\text{C}$ -MMA impregnated samples (see Sect. 4.3.3). Red line marks the interface. The small dimension is 20 mm

**Table 3** Characteristics of the zonation at the ESDRD-Opalinus Clay interface after 2.2 (2) and 4.9 (5) years

	[µm]	Ca	Mg	S	carbo-nation	Mg hydrate
[years]	2	5	2	5	2	5
OPA					Unaltered	
ESDRED					Unaltered	
	-200					
	0					
	300					
	450					
	700					
	1400					
	?					

Empty cells: same characteristics as unaltered material

$+$ ,  $-$ ,  $\checkmark$  represent “enriched”, “depleted”, and “present”, relative to the unaltered Opalinus Clay or cement far from interface. (+): Small enrichment

occupancy obtained from a powder sample carefully scraped from the 0–2 mm interface region in Opalinus Clay (Fig. 12). Other than this, the exchanger appears

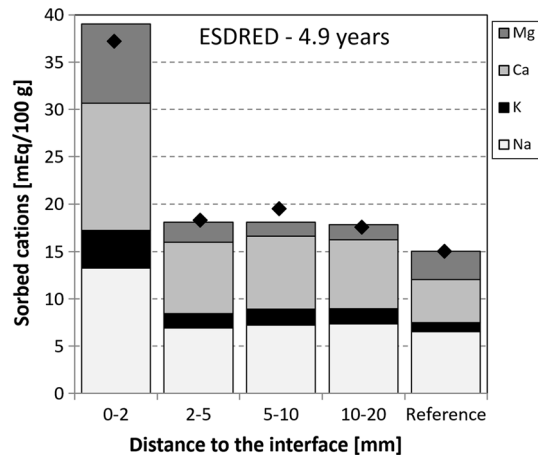


**Fig. 12** CEC (*diamonds*, meq/100 g) and cation occupancy (meq/100 g) on clay exchanger in Opalinus Clay as function of distance from the interface to OPC

undisturbed up to the limit of measurement at 20 mm distance. The unusually large CEC obtained from the sample nearest to the interface may be an artefact from cement material or secondary minerals formed. There is no

CEC/selectivity data available for the 2.2-year sample, but an Mg-enriched zone of comparable width is observed in Opalinus Clay on the Mg element map after 2.2 years (Fig. 11).

#### 4.3.3 Porosity changes across interface region

<sup>14</sup>C-MMA impregnated samples were imaged (Fig. 11, lower images) and treated as described for OPC, here shown as bright areas meaning elevated porosity. Aggregate, MMA-filled cracks, gas voids, and fossil fragments are all segmented and shown in black. The grey scale is different for the claystone side and the concrete side and was optimized for each material to enhance variations at the different average levels. There is no distinct porosity variation near the interface on the concrete side (Fig. 11, left image), and the grey levels are rather similar to deeper parts, but difficult to see in some regions due to the abundance of fine aggregate, also somewhat enhanced by segmentation. There is no porosity variation evident in the claystone as a function of distance from the interface (Fig. 11, right image), only some less porous patches, and more porous cracks that outline bedding. Porosity quantification is still in progress.

#### 4.4 Interpretation of interaction zones

Figure 13 is a summary schematic of the observed alteration near interfaces. In more detail, the features within the cement matrix adjacent to the OPC-Opalinus Clay interface are a Ca-depleted zone with extensive carbonate alteration and a reduced porosity close to Opalinus Clay ( $\sim 1$  mm), followed by a wider sulphur-enriched zone (4–5 mm), before entering almost fully hydrated “normal” OPC. On

the claystone-side of the interface is a conspicuous Mg-enriched zone at 6–8 mm distance, and very minor Ca-rich veinlets representing carbonate precipitation into micro-cracks associated with a borehole-disturbed zone. A more complex zoning pattern in concrete observed after 2.2 years is interpreted to be a result of the low w/c ratio in this sample (from the sealing plug) leading to a two-stage hydration history.

The main features in the cement matrix next to the ESDRED-Opalinus Clay interface are a wider ( $\sim 2$  mm) Ca-depleted zone with some sulphur enrichment towards the unaltered cement matrix. A characteristic feature within the cement matrix is a relatively distinct ( $\sim 2$  mm) Mg-enriched zone, shown to contain Mg-Si-hydrate by Dauzères et al. (2016). A distinct Mg-enrichment is also seen in Opalinus Clay adjacent to concrete (0.5 mm wide).

A distinct de-calcification of the cement matrix seen in both reaction zones (OPC and ESDRED) is the result of a decrease in pH that destabilizes earlier formed Ca-Al-sulphate (ettringite, monosulphate), and these components then re-distribute towards the unaltered cement matrix where they re-precipitate at the prevalent higher pH conditions. Transport is towards the cement interior rather than across the interface into claystone due to the prevalent higher water content/porosity in the former more reactive zone. The carbonate alteration zone is overprinted on the de-calcification zone. This carbonate zone is best confirmed by IR spectroscopy as shown in Fig. 14 where abundant calcite is observed in both types of concrete. The features marked by vertical dashed lines indicate different structures and proportions of Ca-Si-hydrates, and contributions from Mg-hydrates in case of ESDRED. Whereas low levels of carbonate contained in the clinker itself are forming monocarbonate (hydrous Ca-aluminate-carbonate)

**Fig. 13** Summary of observed alteration features near interfaces of OPC and ESDRED with Opalinus Clay (OPA), and some inferred directions of mass transfer

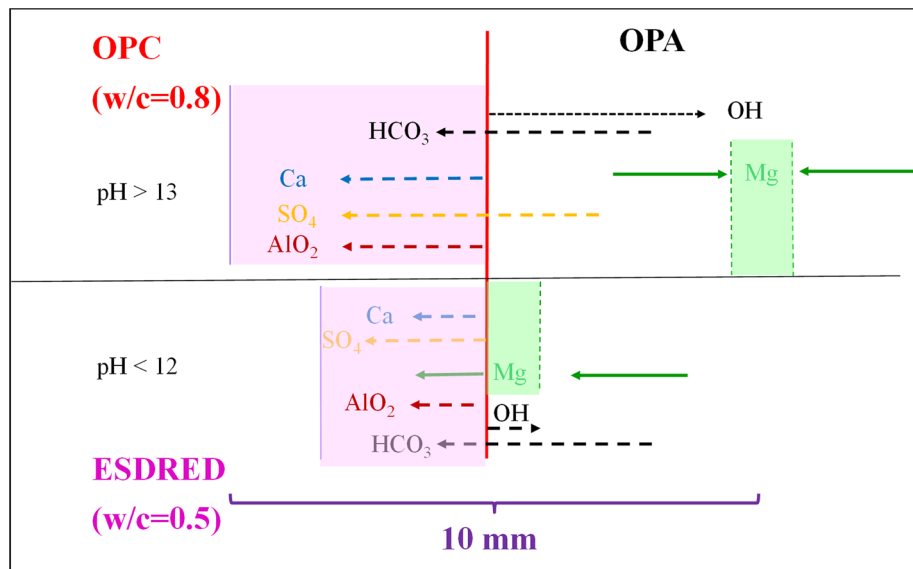
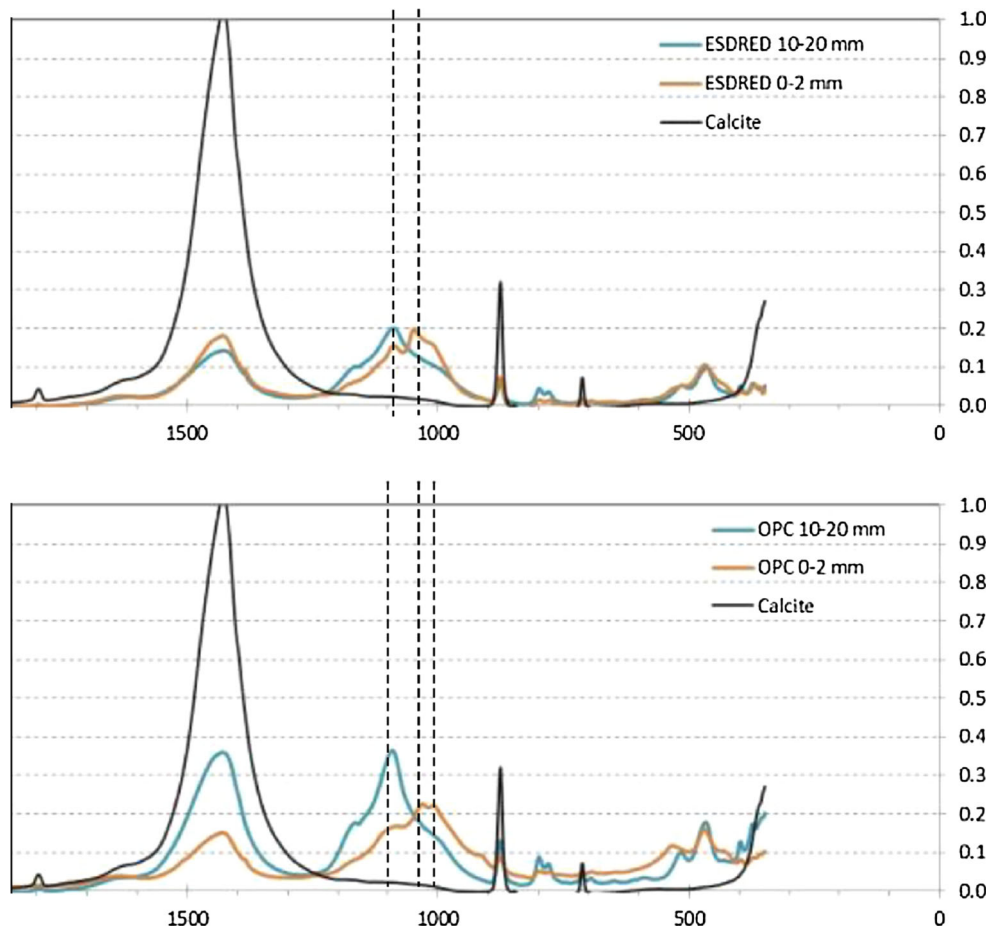


**Fig. 14** IR spectra from alteration zones within cement matrix seen on 4.9-year samples of OPC and ESDRED. X-axis: wave number, Y-axis: intensity normalized to a pure calcite standard. Vertical dashed lines indicate features related to Ca-Si-hydrates and Mg-hydrates



during hydration, the calcite in the alteration zone is formed by in-diffusion of bicarbonate from the claystone pore-water, and calcite is replacing mainly Ca–Si-hydrate, and portlandite during early hydration. This type of carbonation was modelled by Matschei et al. (2007) for OPC and the calculated net reduction in porosity is rather small. The zone with reduced porosity observed in the OPC after 2.2 years (Fig. 9) is thought to be due to carbonation but was likely also affected by the complex mineral dissolution and precipitation reactions that caused the observed Ca-aluminate-sulphate re-distribution.

The very minor alteration of Opalinus Clay next to the concrete interface was unexpected. Except for a distinct Mg-enriched zone detached from the interface (OPC) and a diffuse Mg-enrichment towards the interface (ESDRED), there were no mineralogical changes detected (e.g. by XRD of small bulk samples, by IR spectroscopy, EDAX element mapping). A flux of dissolved Mg towards concrete is expected where the solubility of Mg-phases is very small at high pH. This flux was supplied from the pore-water ( $\sim 350 \text{ mg/l}$ ) and from the clay exchanger ( $\sim 2.6 \text{ g/kg}_{\text{rock}}$ ), representing ca. 12 times the dissolved amount per rock mass. It is therefore plausible that a nearly constant-

concentration boundary was maintained at the interface that supplied Mg to the hydrating cement matrix, initially at a steady rate. This process would have slowed down as hydration proceeded (months), as gradients decreased in the alteration zone and porosity was reduced.

The Mg-enrichment observed in Opalinus Clay adjacent to ESDRED (EDAX, Fig. 10) correlates with an enrichment of Mg on the exchanger determined on mini-samples from 0 to 2 mm of the interface (Fig. 11). Whereas undisturbed Opalinus Clay has a proportion of ca. 10 meq % of Mg on the exchanger, this value was doubled next to the interface, corresponding to ca. 0.5 g/kg<sub>rock</sub>, or 0.05 wt% Mg. Although we did not quantify the EDAX maps, such a small enrichment solely present on the exchanger is not detectable and it is also difficult to reconcile why the exchanger should become enriched in Mg in the absence of a gradient in dissolved concentration of Mg towards the interface. An alternative mechanism is the precipitation of dispersed Mg-hydroxide (e.g. brucite) triggered by an advancing front of somewhat elevated pH. This rise in pH need not be large because the solubility of Mg-hydroxide phases is strongly decreasing with increasing pH. We consider this latter mechanism a more likely

explanation. The amounts may be too small for detection by mineral-specific analysis methods.

The Mg-enriched zone that developed in Opalinus Clay at some distance from the interface to OPC seen after 4.9-years (Fig. 4) is more difficult to explain. Data from the clay exchanger are not entirely conclusive (Fig. 7): Mg is depleted close to the interface (0–5 mm) but at normal or only slightly elevated levels from 5 to 20 mm. The observed enrichment is ca. 1 wt% MgO (EPMA maps, Fig. 4), compared to a maximum amount of ca. 0.24 wt% that could be accommodated on a fully Mg-exchanged clay matrix. It is more plausible to explain this Mg anomaly by precipitation of a Mg-hydroxide (e.g. brucite) in response to an elevated pH front located at this position after 4.9 years. At earlier times, some Mg may have diffused into the cement matrix but to a much lesser degree compared to ESDRED. As a pH front starts to migrate into Opalinus Clay it would push a Mg-precipitation front at its leading edge, and displace and accumulate earlier precipitated Mg-hydroxide deeper into the claystone. This would only require a relatively weak pH front compared to the full potential of a “fresh” OPC pore-water ( $\text{pH} > 13$ ), whereby mineral dissolution of silicates (quartz, clays) would be too slow/too small to induce detectable other mineralogical changes. This leading edge of a dilute pH-plume would then be mainly retarded by the deprotonation of edge sites (illites) with a total site capacity of ca. 0.3 meq/kg<sub>rock</sub>. Most of the pH drop would happen within the cement matrix and Opalinus Clay right next to the interface, presumably by a small amount of silicate dissolution (clays). This proposed process is a hypothesis that is probably best tested by some detailed reactive transport modelling. Some spatially highly-resolved modelling work is in progress to better unravel the observed complex interaction zones, and an attempt to characterize the Mg-zone by  $\mu$ -XRD is in planning, depending on availability of synchrotron beam time.

It appears that at both interfaces—OPC and ESDRED—a sharp pH-drop developed almost immediately right at the interface preventing any further significant OH-attack at the time scale of observation (5 years). It is in fact to be expected that chemical interaction is shifting to the most reactive component, namely the hydrating cement matrix. There, initial water content and porosity are much higher immediately after emplacement of concrete compared to Opalinus Clay, and reaction progress is rapid involving reactive hydrates, sulphates, Ca-aluminates and carbonates. The corollary of this process is that the claystone is being protected from OH-attack mostly by cement-internal processes, enhanced with some influx of Mg, bicarbonate and possibly sulphate from claystone pore-water.

While there is a substantial body of literature that deals with cement leaching (mostly Ca and alkali leaching) the chosen boundary conditions (mostly concrete/mortar/paste against free water) are very different from a cementitious

material in contact with claystone, and thus we did not include a comparison of chemical zoning and textural evolution. We concluded that an analogy based on cement leaching (e.g. Ca leaching) is not of practical relevance for the situation of juxtaposed concrete and claystone.

## 5 Conclusions and outlook

The CI Experiment at the Mont Terri rock laboratory is a long-term technically simple and passive diffusion-reaction experiment between contrasting materials of relevance to engineered barrier systems and the geological near-field for deep disposal of radioactive waste in claystone. Reaction zones at interfaces of Opalinus Clay with two different types of concrete (OPC and “low-pH”/ESDRED) were examined by sampling after 2.2 and 4.9 years. The presence of aggregate grains posed limits to bulk analytical methods and spot analyses, and element mapping had to be used as key tool to characterize rather small-scale reaction zones at the mm and sub-mm scale. OPC and ESDRED mortars (purified quartz) and pastes were emplaced in 2012 (BCI-12–15, Fig. 1) and first sampled in 2015 exactly for the purpose of applying more precise analytical methods with focus on phase identity (analytical work in progress), also including isotopic methods and  $\mu$ -XRD powder techniques (some test results can be found in Dähn et al. 2014). The aim is to provide an as complete as possible mineralogical and geochemical description of the early evolution (0–5 years) of claystone-concrete interfaces that can form a sound basis for a detailed reactive transport modelling interpretation.

A key finding was that the extent of reaction in claystone was minimal for both OPC and ESDRED. The reaction zone within the cement matrix was even larger for the low-alkali cementitious product, despite the fact that pore-water pH is much higher in OPC, and that the water/cement ratio was also higher in OPC compared to ESDRED (0.8 vs. 0.5 in 4.9-year samples). While the absolute potential for OH-release is significantly higher for OPC compared to ESDRED, it appears that the increased reactivity of low-alkali cementitious products pushed by reactive silica (silica fume, silica flower, nanosilica) and set accelerators (aluminate, sulphate, Ca) outperform the effect of mainly a high initial KOH component in OPC that apparently was buffered right at the interface to claystone. Because either a distinct zone of decreased porosity may form (2.2 year, OPC) or porosity is decreasing in cement as hydration progresses in both systems, it may be expected that reaction rates will decrease significantly over time. In fact, the reaction zones observed in the 2.2 and 4.9-year samples of ESDRED already do show quite similar widths, indicative of such a behaviour.

An important conclusion is therefore that substitution of OPC by low-alkali cementitious products is not advantageous or necessary solely for the purpose of minimizing the extent of reaction between claystone and cementitious materials. Substitution of OPC by low-alkali cements may add uncertainty associated with the increased amounts of organic additives, and a less well known engineering performance of such more recently developed products.

A substantial effort has been made in modelling cement-clay interaction (see introduction for some references). Our findings indicate that the following processes and capabilities would need to be part of a more realistic modelling effort: (1) a high spatial resolution (10–100 µm), (2) inclusion of the cement hydration phase/processes, (3) kinetic control of reactions (slow vs. fast reactions), and (4) incorporation of sufficient chemical complexity (Mg phases, Ca–Si-hydrates, Ca–Al-sulphates, carbonates, etc.), although the exact phase identities may not necessarily be a decisive factor. Recent developments in reactive transport codes and efforts in the development of thermodynamic data bases for cement systems (CEMDATA 2016, Thermodynam 2016) appear to make a realistic modelling approach feasible.

A first-order control on system behaviour is the evolution and re-distribution of porosity—and thus permeability—within the reaction zone. Our efforts with  $^{14}\text{C}$ -doped MMA impregnation look promising, but artefacts from sample preparation and data evaluation need to be carefully examined. Ultimately, we would like to know how transport of certain radionuclides (mainly anions) but also water and gas will be affected. A more robust method compared to short-term laboratory experiments might be the implementation of an in situ tracer diffusion test, for example from concrete across an aged interface into claystone, or vice versa. This would provide a direct measure for the

expected decrease of effective diffusion properties as a result of pore clogging (skin effect). Some such efforts (mostly laboratory experiments) were initiated within a European Commission project (CEBAMA 2016).

Planning of a sampling campaign after 10 years of cement-claystone interaction (2017) is initiated. The findings will serve as a robust test for our current state of process understanding, and will extend predictability to several decades (width of reaction zones, porosity evolution) in combination with appropriate modelling.

**Acknowledgements** The authors like to acknowledge the support by the funding organisations of the CI Project and the Mont Terri Consortium—happy birthday and many happy returns. The on-site team of swisstopo supported the field work. Schützeichel GmbH&Co. KG did an excellent job during all drilling campaigns. Bernhard Schwyn (former principle investigator, Nagra) helped to make this project a success and one of the longest-running field experiments at Mont Terri. Bernd Frieg (Nagra) was instrumental for successful drilling during the implementation phase in 2007. The on-site team of the Grimsel Test Site (Toni Baer, Hans Abplanalp, Nagra) provided expertise during the first drilling campaign and sampling of the mock-up barrels. Many colleagues discussed and disputed ideas and analytical methods at various project meetings. We estimate that ca. 40 specialists were involved in this project over the last 12 years. Detailed comments by Jaime Cuevas (UAM, Spain) and Andreas Leemann (EMPA, Switzerland) are kindly acknowledged; they helped to improve the clarity of the arguments and the presentation.

**Open Access** This article is distributed under the terms of the Creative Commons Attribution 4.0 International License (<http://creativecommons.org/licenses/by/4.0/>), which permits unrestricted use, distribution, and reproduction in any medium, provided you give appropriate credit to the original author(s) and the source, provide a link to the Creative Commons license, and indicate if changes were made.

## Appendix

See Figs. 15, 16, 17 and 18 and Table 4.

**Fig. 15** XRD of hydrating OPC paste. A Alite, B belite, C calcite, E ettringite, F ferrite, G gypsum, Ht hydrotalcite, Mc monocarbonate, P portlandite

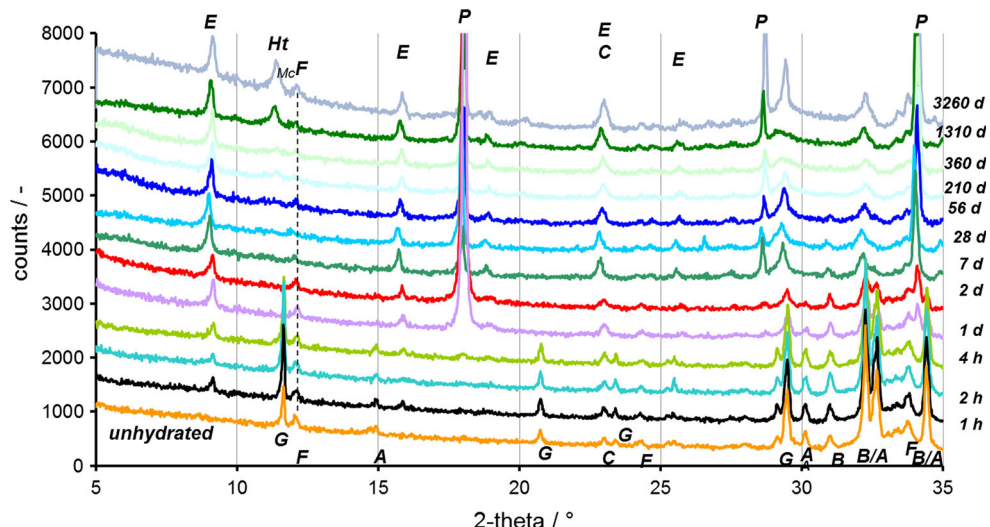


**Fig. 16** TGA/DTG of the unhydrated CEM I 42.5 R HS (used to prepare OPC) and the hydrating OPC paste

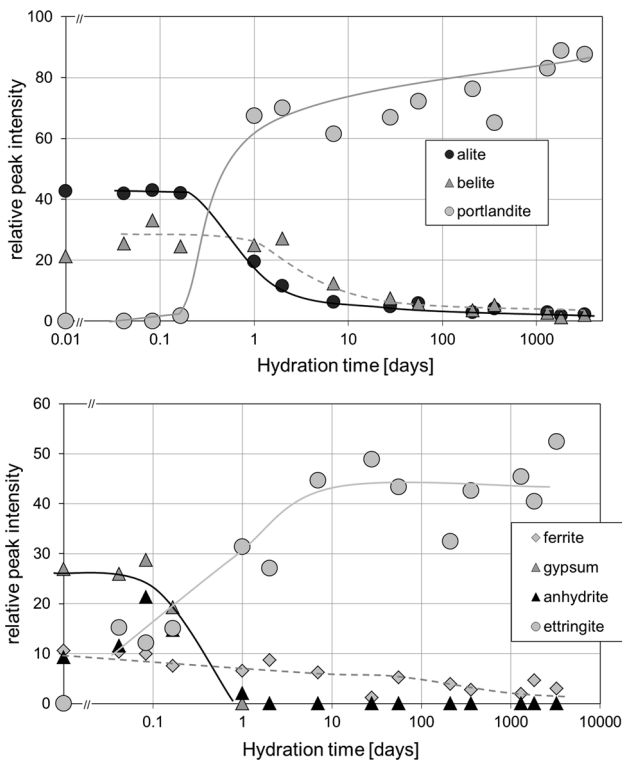
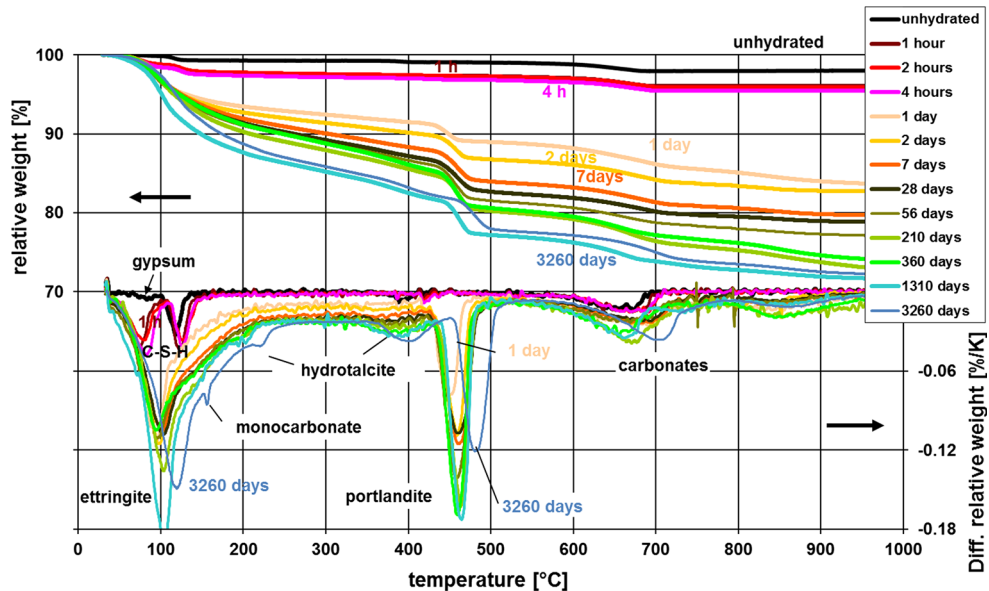


**Fig. 17** Semi-quantitative evaluation of XRD patterns of the solid phase after different hydration times. Lines are intended as eye guides

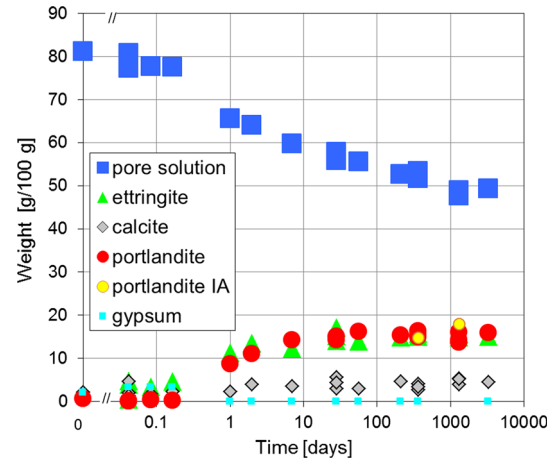


**Fig. 18** Amount of pore-solution, calcite, gypsum, ettringite, and portlandite present during the hydration of OPC as determined by TGA. The weight refers to 100 g of dried solid, i.e. the sample weight before being subjected to TGA. IA determined by image analysis

**Table 4** Measured total concentrations in pore-solutions gained from OPC

Age (days)	Al	Ba	Ca	Cr	K (mmol/l)	Mo	Na	S	Si	Sr	DOC	$\text{OH}^-$ <sup>a</sup>	pH
0.04	0.002	0.0040	24	0.21	137	0.0093	26	66	0.035	0.12	13	105	13.0
0.08	0.002	0.0036	27	0.19	134	0.0088	26	52	0.023	0.13	13	113	13.0
0.17	0.002	0.0031	25	0.17	134	0.0081	26	53	0.028	0.14	13	118	13.0
0.17	0.004	0.0031	24	0.17	–	0.0080	–	52	–	0.14	–	–	–
0.25	0.002	0.0031	25	0.13	136	0.0062	27	54	0.026	0.17	12	128	13.0
1	0.006	0.0038	9.3	0.0003	149	0.0011	44	44	0.047	0.11	12	140	13.1
2	0.021	0.0053	3.6	<	161	0.0003	53	4.9	0.082	0.09	12	214	13.3
7	0.050	0.010	3.1	<	182	<	67	0.7	0.063	0.12	13	249	13.3
28	0.053	0.010	2.4	0.0008	199	<	79	1.1	0.084	0.10	13	269	13.4
28	0.052	0.0098	2.3	0.0008	–	<	–	1.1	0.085	0.10	–	–	–
56	0.019	0.0089	2.3	0.0017	202	0.0003	82	2.1	0.060	0.08	13	272	13.4
207	0.016	0.0088	2.8	0.0035	207	<	89	2.8	0.047	0.11	15	265	13.4
360	0.010	0.0080	1.9	0.0028	208	0.0003	90	3.4	0.051	0.08	13	258	13.3
1310	0.098	0.0056	2.9	<0.004	209	<0.003	90	4.5	0.052	0.12	13	277	13.3
3260	0.163	–	0.72	–	200	–	9.1	6.6	0.053	–	17	264	13.3
Blank	<	<	0.004	<	<	<	2E-3	<	0.002	5E-6	0.3		
DL	0.002	1E-5	3E-4	0.0002	4E-4	0.0003	1E-3	0.01	0.002	3E-6	0.008		

Measured concentrations of Cs, Fe, and Mg were below a detection limit of 0.2, 0.0002 and 0.001 mM, respectively. Measured values for Zn ranged from 0.0003 to 0.001 mM and were in the range of the detection limit

– Not determined

<sup>a</sup> Values for  $\text{OH}^-$  refer to the free concentration as calculated from the measured pH values

## References

- Adler, M. (2001). Interaction of claystone and hyperalkaline solutions at 30°C: A combined experimental and modeling study. Ph.D. Dissertation, (p. 120). Bern, Switzerland: University of Bern.
- Adler, M., & Mäder, U. (1999). Laboratory scoping experiments on high-pH water/shale interaction (CW Experiment). In M. Thury & P. Bossart (Eds.), *Mont Terri Rock Laboratory: Results of the hydrogeological, geochemical and geotechnical experiments performed in 1996 and 1997* (pp. 57–59). Bern: OFEG Report, Geology Serie, No. 23. Federal Office of Topography (swisstopo), Wabern, Switzerland. <http://www.mont-terri.ch>.
- Adler, M., Mäder, U. K., & Waber, H. N. (1999). High-pH alteration of argillaceous rocks: An experimental study. *Swiss Bulletin of Mineralogy and Petrology*, 79, 445–454.
- Adler, M., Mäder, U. K., & Waber, H. N. (2001). Core infiltration experiment investigating high-pH alteration of low-permeability argillaceous rock at 30 °C. In R. Cidu (Ed.), *Proceedings of the 10th International Symposium on Water-Rock Interaction* (pp. 1299–1302). Amsterdam: Balkema Publishers.
- Alonso, J., García-Siñeriz, J. L., Bárcena, I., Alonso, M. C., Fernández Luco, L., García, J. L., Fries, T., Petterson, S., Bodén, A., & Salo, J. P. (2009). *ESDRED, Module 4 (Temporary Sealing Technology) Final Report (Contract FI6 W-CT-2004-508851)*. European Commission, Brussel, Belgium.
- Andersson, M., Ervanne, H., Glaus, M. A., Holgersson, S., Laine, H., Lothenbach B., Puigdomenech, I., Schwyn, B., Snellman, M., Ueda, H., Vuorio, M., Wieland, E., & Yamamoto, T. (2008). *Development of methodology for evaluation of long-term safety aspects of organic cement paste components*. Working Report 2008-28. Posiva Oy, Eurajoki, Finland.
- ANDRA (2005). *Dossier 2005 argile, synthesis: Evaluation of the feasibility of a geological repository in an argillaceous formation. Meuse/Haute-Marne site*. Paris: ANDRA, Agence nationale pour la gestion des déchets radioactifs.
- Bildstein, O., & Claret, F. (2015). Stability of clay barriers under chemical perturbations. In C. Tournassat, C. I. Steefel, I. C. Bourg, & F. Bergaya (Eds.), *Natural and engineered clay barriers* (p. 446). Developments in clay science, vol 6. Amsterdam: Elsevier.
- Bossart, P., Bernier, F., Birkholzer, J., Bruggeman, C., Connolly, P., Dewonck, S., Fukaya, M., Herfort, M., Jensen, M., Matray, J.-M., Mayor, J. C., Moeri, A., Oyama, T., Schuster, K., Shigeta, N., Vietor, T., & Wieczorek, K. (2017). Mont Terri rock laboratory, 20 years of research: introduction, site characteristics and overview of experiments. *Swiss Journal of Geosciences*, 110, doi:10.1007/s00015-016-0236-1.
- Bradbury, M. H., & Baeyens, B. (2000). A generalised sorption model for the concentration dependent uptake of caesium by argillaceous rock. *Journal of Contaminant Hydrology*, 42, 141–163.
- Bradbury, H. M., & Baeyens, B. (2005). Experimental and modelling investigations on Na-illite: Acid-base behaviour and the sorption of strontium, nickel, europium and uranyl. *Nagra Technical Report*, 04-02. Nagra, Wettingen, Switzerland. <http://www.nagra.ch>.
- Bradbury, M. H., Berner, U., Curti, E., Hummel, W., Kosakowski, G., & Thoenen, T. (2014). The Long Term Geochemical Evolution of the Nearfield of the HLW Repository. *Nagra Technical Report*, 12-01. Nagra, Wettingen, Switzerland. <http://www.nagra.ch>.
- CEBAMA. (2016). European Commission Horizon 2020 Research and Training Programme of EURATOM on cement-based materials, properties, evolution, barrier functions. <http://www.cebama.eu/>. Accessed 23 Dec 2016.
- CEMDATA. (2016). Thermodynamic data for hydrated solids in Portland cement system ( $\text{CaO}-\text{Al}_2\text{O}_3-\text{SiO}_2-\text{CaSO}_4-\text{CaCO}_3-\text{Fe}_2\text{O}_3-\text{MgO}-\text{H}_2\text{O}$ ). Administered by Barbara Lothenbach,

- EMPA, Switzerland. <https://www.empa.ch/web/s308/cemdata>. Accessed 23 Dec 2016.
- Dähn, R., Popov, D., Schaub, P., Pattison, P., Grolimund, D., Mäder, U., et al. (2014). In-situ X-ray micro-diffraction studies of heterogeneous interfaces between cementitious materials and geological formations. *Physics and Chemistry of the Earth, Parts A/B/C*, 70, 96–103.
- Dauzères, A., Achiedo, G., Nied, D., Bernard, E., Alahrache, S., & Lothenbach, B. (2016). Magnesium perturbation in low-pH concretes placed in clayey environment—solid characterizations and modelling. *Cement and Concrete Research*, 79, 137–150.
- Dauzères, A., Le Bescop, P., Sardini, P., & Cau Dit Coumes, C. (2010). Physico-chemical investigation of clayey/cement-based materials interaction in the context of geological waste disposal: Experimental approach and results. *Cement and Concrete Research*, 40, 1327–1340.
- De Windt, L., Marsal, F., Tinseau, E., & Pellegrini, D. (2008). Reactive transport modeling of geochemical interactions at a concrete/argillite interface, Tournemire site (France). *Physics and Chemistry of the Earth, Parts A/B/C*, 33, S295–S305.
- De Windt, L., Pellegrini, D., & van der Lee, J. (2004). Coupled modeling of cement/claystone interactions and radionuclide migration. *Journal of Contaminant Hydrology*, 68, 165–182.
- European Commission (2005). *ECOCLAY II, Effects of Cement on Clay Barrier Performance—Phase II, final report (Contract FIKW-CT-2000-00028)*. European Commission, Nuclear Science and Technology.
- Gaboreau, S., Lerouge, C., Dewonck, S., Linard, Y., Bourbon, X., Fialips, C. I., et al. (2012). In-situ interaction of cement paste and shotcrete with claystones in a deep disposal context. *American Journal of Science*, 312, 314–356.
- Gaboreau, S., Prêt, D., Tinseau, E., Claret, F., Pellegrini, D., & Stammose, D. (2011). 15 years of in situ cement–argillite interaction from Tournemire URL: Characterisation of the multi-scale spatial heterogeneities of pore space evolution. *Applied Geochemistry*, 26, 2159–2171.
- Gaucher, E. C., Blanc, P., Matray, J.-M., & Michau, N. (2004). Modeling diffusion of an alkaline plume in a clay barrier. *Applied Geochemistry*, 19, 1505–1515.
- Jenni, A., Mäder, U., Lerouge, C., Gaboreau, S., & Schwyn, B. (2014). In situ interaction between different concretes and Opalinus Clay. *Physics and Chemistry of the Earth, Parts A/B/C*, 70, 71–83.
- Koroleva, M., Lerouge, C., Mäder, U., Claret, F., & Gaucher, E. C. (2011). Biogeochemical processes in a clay formation in situ experiment: Part B—results from overcoring and evidence of strong buffering by the rock formation. *Applied Geochemistry*, 26, 954–966.
- Kosakowski, G., & Berner, U. (2013). The evolution of clay rock/cement interfaces in a cementitious repository for low- and intermediate level radioactive waste. *Physics and Chemistry of the Earth, Parts A/B/C*, 64, 65–86.
- Kosakowski, G., Berner, U., Wieland, E., Glaus, M., & Degueilre, C. (2014). Geochemical evolution of the L/LWL near-field. *Nagra Technical Report*, 14–11. Nagra, Wettingen, Switzerland. <http://www.nagra.ch>.
- Lothenbach, B. (2011). CI experiment: Hydration experiments of OPC, LAC and ESDRED cements: 1 h to 3.5 years. *Mont Terri Technical Note*, TN 2010-75. swisstopo, Seftigenstrasse 264, 3084 Wabern, Switzerland.
- Lothenbach, B. (2013). Hydration of blended cements. In F. Bart, C. Cau-dit-coumes, C. Frizon, & F. Lorente (Eds.), *Cement-based materials for nuclear waste storage* (pp. 33–41). New York: Springer.
- Lothenbach, B., Nied, D., L'Hôpital, E., Achiedo, G., & Dauzères, A. (2015). Magnesium and calcium silicate hydrates. *Cement and Concrete Research*, 77, 60–68.
- Lothenbach, B., Rentsch, D., & Wieland, E. (2014). Hydration of a silica fume blended low-alkali shotcrete cement. *Physics and Chemistry of the Earth, Parts A/B/C*, 70, 3–16.
- Lothenbach, B., & Winnefeld, F. (2006). Thermodynamic modelling of the hydration of Portland cement. *Cement and Concrete Research*, 36, 209–226.
- Mäder, U., & Adler, M. (2005a). Mass balance estimate of cement—clay stone interaction with application to a HLW repository in Opalinus Clay. In *ECOCLAY II, Effects of Cement on Clay Barrier Performance—Phase II, final report (Contract FIKW-CT-2000-00028)* (pp. 188–192). European Commission, Nuclear Science and Technology.
- Mäder, U., & Adler, M. (2005b). A long-term in situ experiment for the interaction of Opalinus Clay with hyperalkaline fluid at the Mont Terri URL (Switzerland). In *ECOCLAY II, Effects of Cement on Clay Barrier Performance—Phase II, final report (Contract FIKW-CT-2000-00028)* (pp. 192–195.). European Commission, Nuclear Science and Technology.
- Marty, N. C. M., Tournassat, C., Burnol, A., Giffaut, E., & Gaucher, E. C. (2009). Influence of reaction kinetics and mesh refinement on the numerical modelling of concrete/clay interactions. *Journal of Hydrology*, 364, 58–72.
- Massat, L., Cuisinier, O., Bihannic, I., Claret, F., Pelletier, M., Masroui, F., et al. (2016). Swelling pressure development and inter-aggregate porosity evolution upon hydration of a compacted swelling clay. *Applied Clay Science*, 124–125, 197–210.
- Matschei, T., Lothenbach, B., & Glasser, F. P. (2007). The role of calcium carbonate in cement hydration. *Cement and Concrete Research*, 37, 551–558.
- Nagra. (2002). Project Opalinus Clay—safety report. Demonstration of disposal feasibility for spent fuel, vitrified high-level waste and long-lived intermediate-level waste (Entsorgungsnachweis). *Nagra Technical Report*, 02-05. Nagra, Wettingen, Switzerland. <http://www.nagra.ch>.
- Nied, D., Enemark-Rasmussen, K., L'Hôpital, E., Skibsted, J., & Lothenbach, B. (2016). Properties of magnesium silicate hydrates (M-S-H). *Cement and Concrete Research*, 79, 323–332.
- Pearson, F. J., Arcos, D., Bath, A., Boisson, J. Y., Fernández, A. M., Gäbler, H. E., Gaucher, E., Gautschi, A., Griffault, L., Hernán, P., & Waber, H. N. (2003). *Mont Terri Project—geochemistry of water in the Opalinus Clay formation at the Mont Terri Rock Laboratory*. Bern: OFEG Report, Geology Serie, No. 5. Federal Office of Topography (swisstopo), Wabern, Switzerland. <http://www.mont-terri.ch>.
- Prêt, D., Sardini, P., Beaufort, D., & Sammartino, S. (2004). Porosity distribution in a clay gouge by image processing of <sup>14</sup>CPolyMethylMethAcrylate (14C-PMMA) autoradiographs. Case study of the fault of St Julien (Basin of Lodève, France). *Applied Clay Science*, 27, 107–118.
- Read, D., Glasser, F. P., Ayora, C., Guardiola, M. T., & Sneyers, A. (2001). Mineralogical and microstructural changes accompanying the interaction of Boom Clay with ordinary Portland cement. *Advances in Cement Research*, 13, 175–183.
- Roosz, C., Grangeon, S., Blanc, P., Montouillout, V., Lothenbach, B., Henocq, P., et al. (2015). Crystal structure of magnesium silicate hydrates (M-S-H): The relation with 2:1 Mg–Si phyllosilicates. *Cement and Concrete Research*, 73, 228–237.
- SCK-CEN (2012). Preparatory safety assessment. Conceptual model description of the reference case. In *External Report of the Belgian Nuclear Research Centre*, ER-215, CCHO—2009-00940000. SCK-CEN, Mol, Belgium. <http://www.sckcen.be>.
- Techer, I., Bartier, D., Boulvais, P., Tinseau, E., Suchorski, K., Cabrera, J., et al. (2012). Tracing interactions between natural argillites and hyper-alkaline fluids from engineered cement paste and concrete: Chemical and isotopic monitoring of a 15-years

- old deep-disposal analogue. *Applied Geochemistry*, 27, 1384–1402.
- Tinseau, E., Bartier, D., Hassouta, L., Devol-Brown, I., & Stammose, D. (2006). Mineralogical characterization of the Tournemire argillite after in situ reaction with concretes. *Waste Management*, 26, 789–800.
- Thermodynam. (2016). Thermochemical and mineralogical tables for geochemical modeling, developed at BRGM, France. <http://thermoddem.brgm.fr/>. Accessed 23 Dec 2016.
- Wieland, E., Lothenbach, B., Glaus, M.A., Thoenen, T., & Schwyn, B. (2014). Influence of superplasticizers on the long-term properties of cement pastes and possible impact on radionuclide uptake in a cement-based repository for radioactive waste. *Applied Geochemistry*, 49, 126–142.